Abstract

This paper reviews the basis of the beam former (BF) and polar correlation (PC) phased array methods and shows that these provide *different* information about axially distributed, non-compact noise sources, which nevertheless satisfy a simple integral relationship. The conventional BF method provides an image of the source PSD, whereas the PC method yields a 'source strength' which is an image of the axial wavenumber transform of the source CSD. However, the BF method can be generalised to provide an image of the source CSD. At first sight the generalised BF method is therefore more useful for diagnostic purposes but the results presented here suggest that the combined effects of resolution and source convection place serious limitations on the source CSD image information. For the same reasons, although the source PSD axial shape can be obtained with the conventional BF method, it cannot yield its absolute level for this type of source. The PC method yields a source strength axial distribution at each 'reference' microphone, which when integrated over the source length, yields the far-field PSD at that reference microphone. Therefore the PC source strength is arguably the more relevant quantity to measure when determining what proportion of the sound at a particular microphone position comes from each region of the jet axis, as a function of radiation angle.

Nomenclature

BF	Beamform or beamformer
C_{qq}	Source CSD
C_{pp}	Far-field CSD or CSM
CSD	Cross-spectral density
CSM	Cross-spectral matrix
c_0	Speed of sound (uniform medium)
d	Jet diameter
f	Frequency
k	ω/c_0 , $= 2\pi St V_J/c_0$ for numerical results
M_c	Source phase convection Mach number = $0.6V_J/c_0$
L_c	Source model coherence length
m	Source PSD model shape parameter
PC	Polar correlation
PSD	Power or Auto spectral density
r_o	Array polar radius
S	PC source strength or intensity per unit length
St	Strouhal number = fd/V_J
Sa	Strouhal number = kL_c/M_c
V_J	Jet velocity
y	Source axial coordinate
y_c	Source model centroid
$p(\omega,\alpha)$	Far-field acoustic pressure, normalised by $4\pi r_o \exp(jkr_o)$
α	Far-field polar angle relative to 90°
β	$k\sin\alpha$

γ	Complex coherence
η	Source axial separation coordinate
ω	Radian frequency

1. Introduction

During the 70's, Phil Morris was conducting research into the role of large-scale structures in the generation of supersonic jet noise at the Lockheed-Georgia Research Labs. The lead author of this paper was working alongside Phil on subsonic jet noise, using a different approach, although at that time there were those who thought that large-scale structures might also play a role in subsonic jet noise. Since that time many others have explored these ideas and we recognise and congratulate Phil on being one of the pioneers in this particular field of aeroacoustics research. Subsequently, some of those researchers have tried to use the coherence properties of the jet near and/or far-field radiation, as measured with phased arrays, to assess the contribution of large-scale structure noise.

To explore that idea this paper has taken a very simple one-dimensional source model with an arbitrary axial coherence length scale but very specific functional models for the source coherence, the source convection and the source strength or intensity and, with the aid of simulation, evaluated the effects of the length scale on the far-field coherence and corresponding beamformed source image. In order to extract a source length scale from the far-field coherence data, it is necessary to generalise the beamformer (BF) process definition. Normally the BF image is a function of the source coordinate but here we need to focus the BF on two axially separated source points. When that separation is zero, the conventional BF image is recovered. For non-zero separations the generalised BF provides an estimate of the source coherence variation with axial separation, that is the length scale. We refer to this as the BF image of the source cross-spectral density (CSD).

Specifically, this paper addresses the questions: (1) what is the relationship between the far-field cross-spectral density matrix (CSM) of jet noise and the source cross spectral density (CSD), characterised by its axial coherence length, convection velocity and intensity variation and (2) what can be resolved from the images generated from the CSM.

The questions are addressed by first describing our understanding of the widely-used beamformer (BF)[1,2,3,4,5,6,7,8] and polar correlation (PC) methods[9,10,11,12,13,14,15] using a consistent approach; second, by introducing a jet noise type line source CSD model for which an analytic far-field CSM expression can be obtained; third, by evaluating these for a realistic combination of jet noise parameters corresponding to a low and medium Strouhal number.

This paper describes developments of on-going work presented previously[16] and was also motivated by Dougherty[17] who showed beamformer results for a single stream jet and remarked on differences in the source image intensity from different parts of the jet with respect to small and large scale noise sources.

2. The source imaging methods

A one-dimensional monopole line source model is utilised for the purposes of this investigation. Extension of this work to 3D and to dipole and quadrupole source distributions is not straightforward but the basic results being established here should provide insight and guidance in that generalisation.

The radiated sound pressure at radian frequency ω due to a monopole line source distribution, measured on a polar arc of radius r_o as shown in Fig. 1, in a uniform medium is given by:

$$p(\omega,\alpha_i) = \int_{-\infty}^{+\infty} q(\omega,y_1) e^{+jky_1 \sin\alpha_i} dy_1 \tag{1}$$

where q is the monopole source strength per unit length, $k=\omega/c_o$ and c_o is the speed of sound. This assumes the far-field approximation for the distance between a point y_1 and a far-field microphone at angle α_i , namely $r_{1i}=r_o-y_1 sin\ \alpha_i$. Here $p(\omega, \alpha_i)$ is the pressure multiplied by $4\pi r_o \exp(jkr_o)$ and similarly for the CSD and PSD below. In principle the analysis is not limited to a polar array and can also be applied to a line array if $p(\omega,\alpha_i)$ is defined as the pressure multiplied by $4\pi r_i \exp(jkr_i)$ where r_i is the distance from the centre of the coordinate system to each microphone.

It follows from Eq. 1 that the CSD of the sound pressure at microphone α_i with that at α_j is:

$$C_{pp}(\omega,\alpha_i,\alpha_j) = \int_{-\infty}^{+\infty}\int_{-\infty}^{+\infty} C_{qq}(\omega,y_1,y_2) e^{+jky_1 \sin\alpha_i - jky_2 \sin\alpha_j} dy_1 dy_2 \tag{2}$$

where C_{qq} is the source CSD. The angle variables (α_i, α_j) are considered as either continuous or discrete variables; in the latter case C_{pp} is often referred to as the cross-spectral density matrix (CSM).

Formally the inverse of this double Fourier transform is:

$$C_{qq}(\omega,y_1,y_2) = \left(\frac{1}{2\pi}\right)^2 \int_{-\infty}^{+\infty}\int_{-\infty}^{+\infty} C_{pp}(\omega,\beta_i,\beta_j) e^{-jky_1\beta_i + jky_2\beta_j} d\beta_i d\beta_j \tag{3}$$

where $\beta_i = k\sin\alpha_i$ in equation (2). This integral yields the source CSD, *if the doubly infinite FT of the far-field CSD in Eq. 3 can be evaluated*. This of course is not the case because $-1 \le \sin\alpha_i \le +1$ and so the integrals can only be evaluated from measurements over a finite range. We therefore can only obtain an estimate of the source distribution for the partial evaluation of this integral as

$$\tilde{C}_{qq}(\omega,y_1,y_2) = \left(\frac{1}{2\pi}\right)^2 \int_{-\beta_{\max}}^{+\beta_{\max}}\int_{-\beta_{\max}}^{+\beta_{\max}} C_{pp}(\omega,\beta_i,\beta_j) e^{-jky_1\beta_i + jky_2\beta_j} d\beta_i d\beta_j \tag{4}$$

where the integrations are limited to $\pm\beta_{\max}$ as explained further below. This is the integral equivalent of the conventional beamformer (BF) method when $y_1=y_2$, that is,

the conventional BF method yields the source PSD. In general the BF method through Eq. 4 can also yield the source CSD, $y_1 \neq y_2$, but with the same integration limits.

Eq. 4 is the first relationship that will be evaluated below, to determine how well the source CSD (C_{qq}), can be resolved from the CSM (C_{pp}), for a given model of C_{qq} .

Anticipating the functional dependence of C_{qq} on a separation variable, the following coordinates are introduced, in the normal way:

$$\eta = (y_1 - y_2); \quad \bar{y} = (y_1 + y_2)/2 \tag{5}$$

where η is the separation coordinate and $\bar{y}$ is the mean coordinate. Eq. 4 then becomes:

$$\tilde{C}_{qq}(\omega, \bar{y}, \eta) = \left(\frac{1}{2\pi}\right)^2 \int_{-\beta_{\max}}^{+\beta_{\max}} \int_{-\beta_{\max}}^{+\beta_{\max}} C_{pp}(\omega, \beta_i, \beta_j) e^{-jk\bar{y}(\beta_i - \beta_j) - jk\eta(\beta_i + \beta_j)/2} \, d\beta_i \, d\beta_j \tag{6}$$

Clearly, in practice the β variable cannot extend to infinity, in fact the maximum aperture of the assumed polar array is -90° ≤ α ≤ 90° and $\beta_{\max} = k$, which defines the maximum resolution limit for C_{qq} .

The form of Eq. 6 suggests a corresponding change in angle coordinates:

$$\beta_{ij}^{+} = \left(\beta_i + \beta_j\right)/2; \quad \beta_{ij}^{-} = \left(\beta_i - \beta_j\right) \tag{7}$$

and Eq. 6 becomes:

$$\tilde{C}_{qq}(\omega, \bar{y}, \eta) = \left(\frac{1}{2\pi}\right)^2 \int_{-\beta_{\max}^{+}}^{+\beta_{\max}^{+}} e^{-jk\eta\beta_{ij}^{+}} \, d\beta_{ij}^{+} \int_{-\beta_{\max}^{-}}^{+\beta_{\max}^{-}} C_{pp}(\omega, \beta_{ij}^{+}, \beta_{ij}^{-}) e^{-jk\bar{y}\beta_{ij}^{-}} \, d\beta_{ij}^{-} \tag{8}$$

As noted above this is the integral equivalent of the basic beamformer (BF) method when $\eta=0$. Now the finite aperture would give $\beta_{\max}^{+} = k$ and $\beta_{\max}^{-} = 2k$.

Turning to the Polar Correlation (PC) method, we first note that Eq. 2 in these new spatial and angular coordinates becomes:

$$C_{pp}(\omega,\beta_{ij}^{+},\beta_{ij}^{-}) = \int_{-\infty}^{+\infty} e^{+jk\bar{y}\beta_{ij}^{-}}\, d\bar{y} \int_{-\infty}^{+\infty} C_{qq}(\omega,\bar{y},\eta) e^{+jk\eta\beta_{ij}^{+}}\, d\eta \tag{9}$$

The far-field PSD follows directly from Eq. 9 and is given by:

$$\begin{aligned} C_{pp}(\omega,\beta_{ij}^{+}=\beta_i,\beta_{ij}^{-}=0) \equiv S_{pp}(\omega,\beta_i) &= \int_{-\infty}^{+\infty} d\bar{y} \int_{-\infty}^{+\infty} C_{qq}(\omega,\bar{y},\eta) e^{+jk\eta\beta_i}\, d\eta \\ &= \int_{-\infty}^{+\infty} S(\omega,\bar{y},\beta_i) d\bar{y} \end{aligned} \tag{10a}$$

where we define the 'source strength' per unit length for the observer at angle α_i (defined by $\beta_i = k\sin\alpha_i$) as:

$$S(\omega,\bar{y},\beta_i) = \int_{-\infty}^{+\infty} C_{qq}(\omega,\bar{y},\eta) e^{+jk\eta\beta_i}\, d\eta \tag{10b}$$

S is a generalised form of the source strength per unit length that forms the basis of the polar correlation (PC) method. Eq. 10a states that the far-field PSD is equal to the axial wavenumber transform of the source CSD with respect its axial separation, evaluated with wavenumber β_i and integrated over the source length. In terms of this source strength the far-field PSD is simply the source strength integrated over the source length (the RHS of Eq. 10a). Thus with adequate information on the source CSD, C_{qq}, the far-field PSD can be quantitatively evaluated in terms of the source strength distribution with Eq. 10a, e.g. how much sound comes from one part of the distribution *versus* another at a particular angle α_i. Thus the PC method provides a simple direct expression for the far-field PSD, S_{pp}, as an integral of the source distribution, $S(\omega,\bar{y},\beta_i)$.

The second relationship to be evaluated below is the one corresponding to Eq. 9 for the far-field CSD, written in terms of the source strength, which is:

$$\begin{aligned} C_{pp}(\omega,\beta_{ij}^{+},\beta_{ij}^{-}) &= \int_{-\infty}^{+\infty} e^{+jk\bar{y}\beta_{ij}^{-}}\, d\bar{y} \int_{-\infty}^{+\infty} C_{qq}(\omega,\bar{y},\eta) e^{jk\eta\beta_{ij}^{+}}\, d\eta \\ &= \int_{-\infty}^{+\infty} S(\omega,\bar{y},\beta_{ij}^{+}) e^{+jk\bar{y}\beta_{ij}^{-}}\, d\bar{y} \end{aligned} \tag{11a}$$

where the source strength is:

$$S(\omega,\bar{y},\beta_{ij}^{+}) = \int_{-\infty}^{+\infty} C_{qq}(\omega,\bar{y},\eta)e^{jk\eta\beta_{ij}^{+}}\,d\eta \tag{11b}$$

and is effectively the same as the quantity defined in Eq. 10b.

The inverse of Eq. 11a, which is

$$S(\omega,\bar{y},\beta_{ij}^{+}) = \frac{1}{2\pi}\int_{-\infty}^{+\infty} C_{pp}(\omega,\beta_{ij}^{+},\beta_{ij}^{-})e^{-jk\bar{y}\beta_{ij}^{-}}\,d\beta_{ij}^{-} \tag{12}$$

shows that the single FT of the far-field CSD w.r.t separation in the sine of the microphone angles gives the same quantity, *S*, that is required for the axial distribution of the far-field PSD, given by Eq. 10b. It is the second relationship that will be evaluated below, to determine how well this source strength can be resolved from the CSM (C_{pp}).

We can now establish a link between the BF and PC methodology. The conventional BF method uses a (discretised) form of Eq. 8 with, necessarily, a finite aperture to compute the BF source image of the source PSD defined by:

$$\tilde{C}_{qq}(\omega,\bar{y},\eta=0) = \left(\frac{1}{2\pi}\right)^{2}\int_{-\beta_{\max}^{+}}^{+\beta_{\max}^{+}} d\beta_{ij}^{+}\int_{-\beta_{\max}^{-}}^{+\beta_{\max}^{-}} C_{pp}(\omega,\beta_{ij}^{+},\beta_{ij}^{-})e^{-jk\bar{y}\beta_{ij}^{-}}\,d\beta_{ij}^{-} \tag{13a}$$

where the maximum practical aperture gives as above $\beta_{\max}^{-} = 2k$ with $\beta_{\max}^{+} = k$.

The PC method computes the source strength using the finite aperture form of Eq. 12 and is a function of the mean spatial coordinate and the mean of the sine angles:

$$\tilde{S}(\omega,\bar{y},\beta_{ij}^{+}) = \frac{1}{2\pi}\int_{-\beta_{\max}^{-}}^{+\beta_{\max}^{-}} C_{pp}(\omega,\beta_{ij}^{+},\beta_{ij}^{-})e^{-jk\bar{y}\beta_{ij}^{-}}\,d\beta_{ij}^{-} \tag{13b}$$

Comparing the above two equations, it can be seen that the BF source image given by Eq. 13a is simply the integral of the PC source strength, $S(\omega,\bar{y},\beta_{ij}^{+})$, given by Eq. 13b, over the finite aperture, w.r.t β_{ij}^{+}.

3. The CSD source model

The two-point source CSD, C_{qq}, is by definition the square root of the product of the source PSD at each point, times its coherence, γ

$$C_{qq}(\omega,y_1,y_2) = \left(C_{qq}(\omega,y_1,y_1)\right)^{1/2}\left(C_{qq}(\omega,y_2,y_2)\right)^{1/2}\gamma(\omega,y_1-y_2) \tag{14}$$

The model for the square root of the source PSD is given by[18]:

$$\left(C_{qq}(\omega, y, y)\right)^{1/2} = \sqrt{y^{m-1} e^{-my/y_c}}; \quad y \geq 0, \quad m = 3 \tag{15a}$$

where y_c is the centroid and the shape parameter $m=3$ is selected to permit the far-field CSD to be obtained analytically. Examples of this source PSD model are shown in Fig. 2a for values of y_c that are used below.

For the coherence model, the Fourier transform of a widely accepted two-point cross-correlation function model used by Tam *et al*[19] and Karabasov *et al* [20]is employed here (see Appendix A for details):

$$\gamma(y_1 - y_2) = e^{-|y_1 - y_2|/L_c - ik(y_1 - y_2)/M_c} \tag{15b}$$

where L_c is the coherence length and M_c the convection velocity. In the examples that follow an arbitrary jet diameter, d, jet velocity V_J and hence a Strouhal number, $St = fd/V_J$ are introduced to determine typical values of y_c and L_c. Another Strouhal number, $Sa = kL_c/M_c$, arises in the Eq. 17 below.

From Eqs. (14-15), the final expression for the source CSD in terms of the mean and separation coordinates is

$$C_{qq}(\omega, \bar{y}, \eta) = \left(\bar{y}^2 - (\eta/2)^2\right) e^{-m\bar{y}/y_c} e^{-|\eta|/L_c - ik\eta/M_c}; \quad \bar{y} \geq 0, \quad m = 3 \tag{16}$$

When Eq.16 is substituted into Eq. 11a, the double integration can be performed analytically (but only with $m=3$) and yields:

$$C_{pp}(\omega, \beta_{ij}^+, \beta_{ij}^-) = 8\left(\frac{A+B}{A^3(A+2B)^2}\right) + 8\left(\frac{A+B^*}{A^3(A+2B^*)^2}\right) \tag{17a}$$

where:

$$A = m/y_c\left(1 - jy_c\beta_{ij}^-/m\right); \qquad B = 1/L_c\left(1 + j\left(kL_c/M_c\right)\left(1 - M_c\beta_{ij}^+/k\right)\right) \tag{17b}$$

The derivation of Eq. 17 is outlined in Appendix B.

Thus the far-field CSD can be evaluated exactly with Eq. 17 as a function of $\beta_{ij}^- \Rightarrow \beta_i$ with $\beta_{ij}^+ = 0$ that is, with one microphone fixed at 90°, which is called the reference microphone. This is used below as the input to the two different transforms of the CSM that provide (simulated) estimates or images of the source characteristics

which are then compared directly with the analytic source CSD defined by Eqs.14-16. Examples of the far-field PSD directivity of this model, with $\beta_{ij}^{-} = 0, \beta_{ij}^{+} = k\sin\alpha \equiv -k\cos\theta$, where θ is the intake angle, are shown in Fig. 2b for a source convection Mach number M_c = 0.6 and various values of the source axial coherence length L_c, which are explained below. The directivity clearly asymptotes to the inverse second power of the Doppler factor with increasing L_c.

The far-field CSD modulus (normalised by the PSD at the reference angle) and the far-field coherence modulus are shown in Figs. 2c & 2d, with the CSD phase in Fig. 2e. Clearly neither the CSD or coherence modulus is a strong function of L_c and counter-intuitive trends are evident, for example the far-field coherence modulus reduces as the source coherence length is increased.

Taking the compact limit for the source parameters in Eq. 17 ($S_a \to 0$, $L_c \to 0$) and substituting into Eq. 13b gives the following expression for the PC source strength, if we assume an infinite aperture ($\beta_{\max}^{-} \to \infty$):

$$S(\omega, \bar{y}, \beta_{ij}^{+}) = 2L_c \bar{y}^{m-1} e^{-m\bar{y}/y_c} \tag{18a}$$

That is the source strength is independent of β_{ij}^{+}, i.e. unidirectional, and is proportional to the coherence length. If that expression for the source strength is substituted into Eq. 13a for the BF source image we obtain for a finite aperture in the mean sine angle:

$$C_{qq}(\omega, \bar{y}, \eta = 0) = (\beta_m^{+} / \pi) 2L_c \bar{y}^{m-1} e^{-m\bar{y}/y_c} \tag{18b}$$

Thus provided the source CSD is compact and an infinite aperture is assumed, the BF and PC methods give the same result for the axial source distribution, differing only by the aperture factor β_m^{+} / π. For non-compact jet noise distributions, we have to resort to numerical evaluation.

4. Extracting the source CSD from a double transform of the CSM (BF method)

Examples are given of the numerical evaluation of the BF image of the source CSD, $\tilde{C}_{qq}$, given by the double transform in Eq. 6, in the form:

$$\tilde{C}_{qq}(\omega,\bar{y},\eta)=\left(\frac{1}{2\pi}\right)^2\int_{-\beta_{\max}}^{+\beta_{\max}}\int_{-\beta_{\max}}^{+\beta_{\max}} C_{pp}(\omega,\beta_i,\beta_j)e^{-j\bar{y}(\beta_i-\beta_j)-j\eta(\beta_i+\beta_j)/2}\,d\beta_i\,d\beta_j \qquad (19)$$

where the axial coordinate has been transformed as defined by Eq. 5 and the infinite limits have necessarily been replaced by finite limits corresponding to the array aperture. In practice this limit cannot exceed *k* but values larger than this are considered below to demonstrate trends and verify the computation method.

In this and the next section, the computations have been conducted with a polar array of aperture 180° (the maximum) and microphone spacing of 1°. This aperture and spacing are not too far removed from some of those being used in practice, although usually in the form of a linear array[21].

Imaging the Source PSD

Setting the separation coordinate η=0 in Eq. 19, the BF image of the source PSD is first evaluated with a large (unrealistic) value of the aperture of $\beta_{max}= 10k$ to indicate that the BF image tends towards the correct source PSD as the aperture tends to infinity. The other parameter values are *St = 0.1*, $V_J/\,c_o=1$, $y_c/d=13$, $M_c=0.6\,V_J/\,c_o$ and a range of axial coherence lengths centred on a nominal value (except in Figs. 6-9 where it is the first value) given by $L_c/d= y_c/8d$, which has been obtained from the LES results of Karabasov[20]; details are given in Appendix A. The BF image strength increases with *increasing* coherence length, converging on the 'True PSD' result - given by Eq. 16 - shown as the black line in Fig. 3a. Presumably if the aperture were to be increased further the BF images would converge to the true PSD independent of L_c. However, if a realistic value of $\beta_{max}= k$ is used for the integration limits in Eq. 19, the BF images differ quite significantly from the true PSD as shown in Fig. 3b, the PSD image maximum being less than 20% of the true value. Furthermore the large aperture trend shown in Fig. 3a is replaced by a non-uniform behaviour, the BF image maximum coincidentally being for $L_c/\lambda = 0.16$ corresponding to the nominal value $L_c/y_c = 1/8$ (see Eq. A.2). However if each BF image is normalised by its peak value, the agreement in shape is very good, as shown in Fig. 3c. Figs. 4a & 4b show similar results for *St=1*, although now the strongest BF image corresponds to the smallest L_c value. Much stronger BF image results are obtained for a supersonic jet for which the convection velocity is also supersonic, $V_J/\,c_o=2$, but the mismatch between the BF image and the true PSD is significantly reduced, as shown in Fig. 5 for *St = 0.1* the trend with L_c being similar to that for large aperture in Fig. 3a. This distinct difference between BF images for subsonic and supersonic convection Mach numbers (for a realistic aperture) is also a noticeable feature of the CSD BF images, discussed below, and it is suggested here that the BF image limitations for the PSD and CSD are due to the same problem of phase resolution.

These results have been indirectly confirmed by analytically integrating Eq. 19 w.r.t. $\bar{y}$ to obtain the integral of the source PSD over the source length as a function of aperture and the jet noise model parameters. Apart from convection Mach number, clearly aperture is a significant parameter and considerably smaller aperture array

apertures are often used in practice. It may be possible to improve the resolution of the source PSD with techniques proposed Brooks[22] and others, e.g. Sijtsma[23].

Imaging the Source CSD or coherence

Using the same parameter values as in Fig. 3, Eq. 19 is evaluated again but now with a non-zero separation,η, to give a generalised normalised BF image of the source CSD, first with a large (unrealistic) value of the aperture of $\beta_{max}= 10k$ to indicate that the correct source CSD can be recovered as the aperture tends to infinity, as shown in Fig. 6a for the normalised CSD modulus and the phase in Fig. 6b. However with a realistic aperture Fig. 7a shows that the BF image of the CSD modulus is limited by resolution, even when the coherence length is significantly greater than a half a wavelength. The BF image of the phase in Fig. 7b suggests a contributory factor, in that the phase of the true CSD, which is controlled by the convection velocity, is not properly resolved by the BF image phase except for the largest coherence length.

If the convection velocity is omitted from the model, it is interesting to see in Fig. 8 that the BF image modulus resolves the source CSD modulus in the expected way, so clearly it is this parameter which is preventing the BF image from resolving the CSD, when the coherence length exceeds a half a wavelength. (In this zero convection velocity case the phase of the source CSD is zero.)

When the convection velocity is increased, as before, to a supersonic value, Fig. 9a shows that the BF image of the source CSD modulus responds to an increasing coherence length. However, it is still not accurately resolving this length scale, despite the apparent good resolution of the phase in Fig. 9b for the largest coherence length.

5. Extracting the source strength from a single transform of the CSM (PC method)

Examples are given of the numerical evaluation of the source strength given by the single transform in Eq. 13b, in the form of a finite aperture integration:

$$\tilde{S}(\omega, \bar{y}, \beta_{ij}^{+}) = \frac{1}{2\pi} \int_{-\beta_{\max}^{-}}^{+\beta_{\max}^{-}} C_{pp}(\omega, \beta_{ij}^{+}, \beta_{ij}^{-}) e^{-jk\bar{y}\beta_{ij}^{-}} \, d\beta_{ij}^{-} \tag{20}$$

and results are compared with the exact analytic results.

Using the same parameter value set as in the previous section and starting with an unrealistically large aperture corresponding to $\beta_{max}= 10k$ and $\beta_{ij}^{+} = 0$ (i.e. 90º to the jet or line source axis) the numerical integration of Eq. 20 yields the results shown in Fig. 10a for *St=0.1*, all of which indistinguishable from the corresponding analytic result (which itself is varying with the coherence length, unlike the BF results). The corresponding results for an aperture $\beta_{max}= k$ in Fig. 10b are very similar with the exception of the largest coherence length, where the PC image is unable to resolve the axial 'ripple', presumably because it is varying rapidly over half a wavelength. The trends are similar at the higher Strouhal number, *St=1*, in Fig. 11. However, at the supersonic velocity condition for *St=0.1* the largest coherence length is now greater

than a wavelength and the PC image in Fig. 12 is able to resolve the rapid axial variation (ripple). This axial variation characteristic of the PC image might be a useful indicator of larger-than-expected coherence length scales in supersonic jets.

6. Conclusions

This paper has reviewed the basis of the beam former (BF) and polar correlation (PC) phased array methods and has shown that these provide *different* information about axially distributed jet noise type sources. The conventional far-field BF source image is derived from the Fourier transform of the far-field CSD (or CSM), w.r.t to the axial coordinate, averaged over the array aperture and has been shown to be equal to the source PSD for an infinite aperture. The PC source strength for each reference microphone, has been identified as the Fourier transform of the source CSD with respect to axial separation. The PC image at each reference angle is the Fourier transform w.r.t. the axial coordinate of the far-field CSD (or CSM). It follows that BF image is the integral or average of the PC source image over all reference angles.

To assess these phased array methods for the purposes of determining length scales in a jet noise type source, the conventional BF has been extended. The conventional BF image of a line source is a function of the one source coordinate but here we have extended the BF method to focus on two axially separated source points. When that separation is zero, the conventional BF image is recovered and hence the source PSD. For non-zero separation the extended or generalised BF method for an infinite aperture, yields the source CSD and its variation with axial separation.

To help understand these two phased array methods in more detail, in particular the generalised BF method, we have assumed a one-dimensional source having a coherence that combines previously published models for the variation in source coherence with axial separation, including convection, and for the PSD axial variation in source strength or intensity. With the aid of this model and numerical simulation, it has been possible to evaluate the effects of the length scale on the far-field coherence and the derived BF image of the source CSD.

Fortunately, the simulations have been underpinned by an analytic expression that we have derived for the far-field CSD radiated by this source CSD model, with the constraint that the source has a particular value of the shape parameter for the source PSD axial variation. This has enabled comparison of all the numerically derived results with the ‘true’ source PSD and CSD.

The simulations in this paper have been confined to a polar phased array with the maximum aperture of 180° and 1° microphone spacing. These are not unrealistic array parameters, although in practice the arrays are usually linear rather than polar and the aperture is necessarily somewhat smaller.

From these simulations, it has been shown that the for subsonic jet convection Mach numbers, the axial coherence length scale cannot be satisfactorily resolved from the generalised BF image of the CSD, even with the maximum polar array aperture of 180 degrees. The same is true, strictly speaking, for supersonic convection Mach numbers, although trends in the length scale can be detected. The reason appears to be that far-field BF (complex) coherence data cannot accurately resolve the source phase

variation with separation caused by a subsonic convection velocity. When a supersonic convection velocity is assumed, the phase variation is resolved with reasonable accuracy. However, although the image modulus variation with axial separation exhibits the correct trend, it still does not provide the correct quantitative variation. Our main conclusion is that far-field coherence data can be used with the generalised BF to obtain qualitative estimates of the large-scale structure noise contribution but only for supersonic convection velocities.

The above findings have implications for the conventional BF, which is widely used for diagnostic purposes on aeroacoustic sources, including jet noise. It has been shown that the combined effects of resolution and source convection place significant limitations on the absolute level of the BF image of the source PSD, although its axial shape is almost fully recovered.

The PC method yields a source strength image at each reference microphone (only 90° is considered here, i.e. normal to the jet axis) which when integrated over the source length, yields the far-field PSD at that reference microphone. Therefore the PC source strength is the most reliable and relevant quantity to measure when addressing the question: what proportion of the sound at a particular microphone position comes from this region of the jet axis?

The PC source strength image is much less affected by resolution and convection effects, except for large length scales at subsonic convection Mach numbers, but even then it provides a good average of the axial variation in source strength. In general it closely follows ‘true’ source strength over a wide range of length scales and the source strength level does vary with coherence length in a systematic way. It might therefore be possible to extract length scale information from the PC image of the source strength.

Ideally more work should be done to improve the realism of these simulations. For example previous measurements and also LES data show that length scale varies almost linearly with distance downstream of the jet nozzle, whereas here we have assumed a constant length scale corresponding to the axial position defined by the Strouhal number. That linear variation needs to be incorporated in our model, along with simulated errors and a range of realistic apertures.

7. Acknowledgements

Funding of this work by the Aeroacoustics Research Consortium is gratefully acknowledged.

Appendix A

Axial coherence length scale estimation

For the purposes of this study we have used the axial separation dependence of the 'fine-scale' jet noise source two-point space-time correlation model proposed by Tam & Auriault[19], for which the corresponding coherence takes the form:

$$\gamma(y_1 - y_2) = e^{-|y_1 - y_2|/L_c + ik(y_1 - y_2)/M_c} \tag{A.1}$$

where the coherence length scale, L_c, is expressed as $\bar{u}\tau_s$ in Ref. 3; $\bar{u}$ is the convection velocity, denoted here by $c_O M_C$, and τ_s is the characteristic decay time. Approximate values for these parameters were chosen by fitting to previous two-point measurements, in Ref. 3, but subsequently τ_s and other parameters were adjusted to obtain the best fit to predicted far-field noise spectra. More recently Karabasov *et al*[20] have been able to provide better direct estimates of $L_c = \bar{u}\tau_s$ by fitting the above type of model to two-point space-time correlations of the fluctuating unit Reynolds stress obtained from an LES solution and concluded that for a single stream un-heated jet τ_s varies almost linearly with the axial distance downstream of the nozzle. Their data can be represented, to a good approximation, as:

$$\frac{L_c}{d} = \frac{1}{8}\frac{\bar{y}}{d} \tag{A.2}$$

where $\bar{y}$ is the axial distance downstream of the nozzle and *d* is the nozzle diameter.

In the numerical calculations presented in this paper, L_c has been assumed to be a constant for a given Strouhal number and its value obtained from Eq. A2 to obtain a 'nominal' value for a given axial source position. The value of $\bar{y}$ has been obtained from previous source location measurements, e.g. for *St=0.1,* $\bar{y}$ *= 13d* and for St=1, $\bar{y}$ *= 5d.* In general numerical results in Sections 4 & 5 are presented for a range of L_c spanning the nominal value.

Appendix B

Derivation of analytic far-field CSD

Eq. (11a) gives the far-field CSD as a double Fourier transform of source CSD , which is

$$\begin{aligned} C_{pp}(\omega,\beta_{ij}^{+},\beta_{ij}^{-}) &= \int_{-\infty}^{+\infty} e^{+j\bar{y}\beta_{ij}^{-}}\, d\bar{y} \int_{-\infty}^{+\infty} C_{qq}(\omega,\bar{y},\eta) e^{j\eta\beta_{ij}^{+}}\, d\eta \\ &= \int_{-\infty}^{+\infty} S(\omega,\bar{y},\beta_{ij}^{+}) e^{+j\bar{y}\beta_{ij}^{-}}\, d\bar{y} \end{aligned} \tag{B.1}$$

To show how Eq. (17) has been obtained, the source PSD model given by Eq. (15a) has to be re-written as

$$\left(C_{qq}(\omega,y,y)\right)^{1/2} = H(y)\sqrt{y^{m-1}e^{-my/y_c}}\,; \quad m=3 \tag{B.2}$$

where *H()* is the Heaviside step function. Substituting Eq. (B.2) and Eq. (15b) into Eq.(14) gives

$$C_{qq}(\omega,y_1,y_2) = H(y_1)\sqrt{y_1^{m-1}e^{-my_1/y_c}}\,H(y_2)\sqrt{y_2^{m-1}e^{-my_2/y_c}}\,e^{-|y_1-y_2|/L_c - ik(y_1-y_2)/M_c} \tag{B.3}$$

or in mean/separation coordinates(with m=3)

$$C_{qq}(\omega,\bar{y},\eta) = H\left(\bar{y}+\eta/2\right)H\left(\bar{y}-\eta/2\right)\left(\bar{y}^2-\left(\eta/2\right)^2\right)e^{-m\bar{y}/y_c}e^{-|\eta|/L_c - ik\eta/M_c} \tag{B.4}$$

Substitution of Eq. (B.4) into Eq. (B.1) gives

$$\begin{aligned} &C_{pp}(\omega,\beta_{ij}^{+},\beta_{ij}^{-}) = \\ &\int_{-\infty}^{+\infty} e^{+j\bar{y}\beta_{ij}^{-}}\, d\bar{y} \int_{-2\bar{y}}^{+2\bar{y}} H^2(\bar{y})\left(\bar{y}^2-\left(\eta/2\right)^2\right)e^{-m\bar{y}/y_c}e^{-|\eta|/L_c - ik\eta/M_c}e^{j\eta\beta_{ij}^{+}}\, d\eta \end{aligned} \tag{B.5}$$

where the integration limits for η have been modified by the Heaviside functions. Integration with respect to η gives in effect the PC source strength

$$S(\omega,\bar{y},\beta_{ij}^{+}) =$$
$$H^2(\bar{y})e^{-m\bar{y}/y_c}\,2\,\mathrm{Re}\left(\frac{\bar{y}^2}{B}\left(1-e^{-2\bar{y}B}\right)-\frac{1}{2B^3}\left(1-e^{-2\bar{y}B}\left(1+2\bar{y}B+2\bar{y}^2B^2\right)\right)\right) \tag{B.6}$$

where

$$B = 1/L_c\left(1+j\left(kL_c/M_c\right)\left(1-M_c\beta_{ij}^{+}/k\right)\right) \tag{B.7}$$

Substituting Eq. (B.7) into Eq. (B.1) gives

$$C_{pp}(\omega,\beta_{ij}^{+},\beta_{ij}^{-}) = \int_{-\infty}^{+\infty} e^{+j\bar{y}\beta_{ij}^{-}} e^{-m\bar{y}/y_c} H^2\left(\bar{y}\right) \tag{B.7}$$
$$2\,\mathrm{Re}\left(\frac{\bar{y}^2}{B}\left(1-e^{-2\bar{y}B}\right)-\frac{1}{2B^3}\left(1-e^{-2\bar{y}B}\left(1+2\bar{y}B+2\bar{y}^2B^2\right)\right)\right)d\bar{y}$$

The final integration then yields Eq. (17).

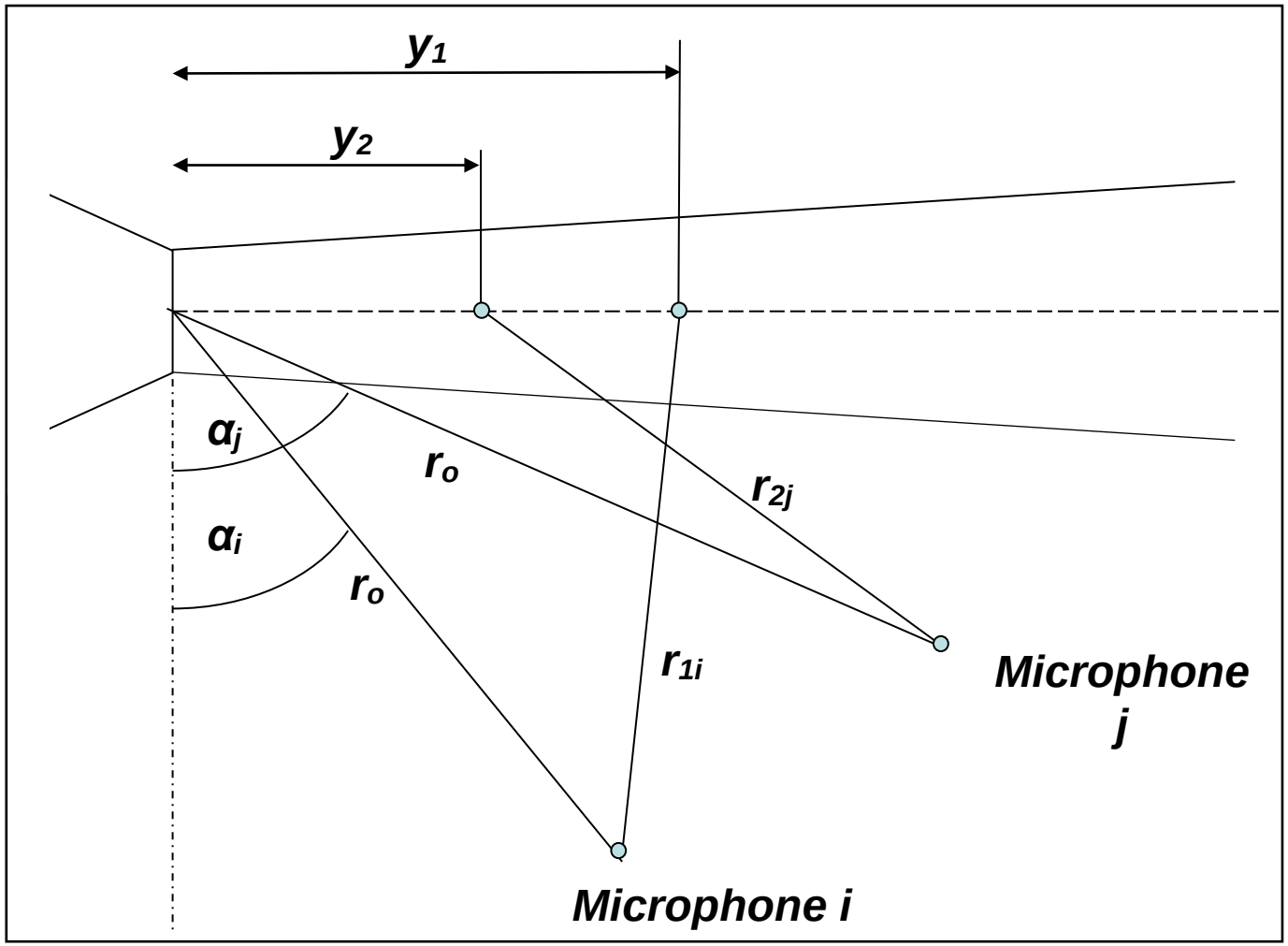

Figure 1: Monopole 1D line source model, with microphones on polar arc

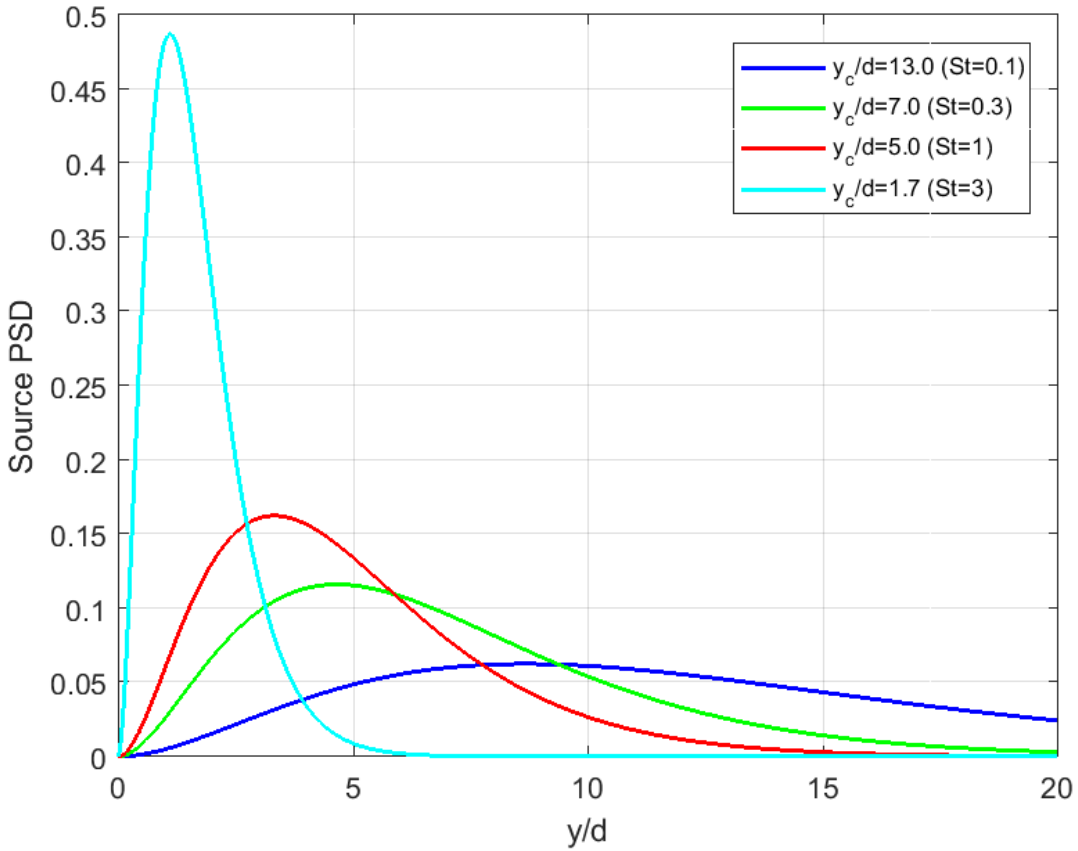

Figure 2a: Source PSD model (m=3)

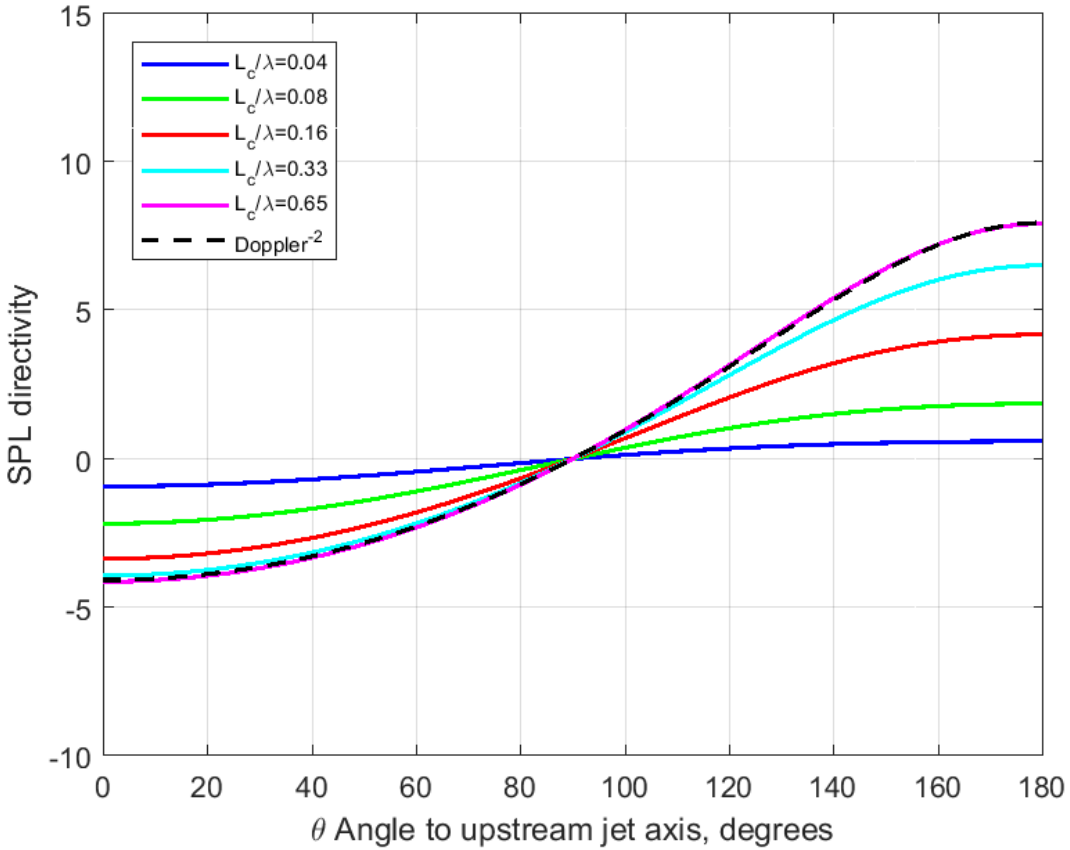

Figure 2b: Far-field PSD directivity, St = 0.1, Mc=0.6.

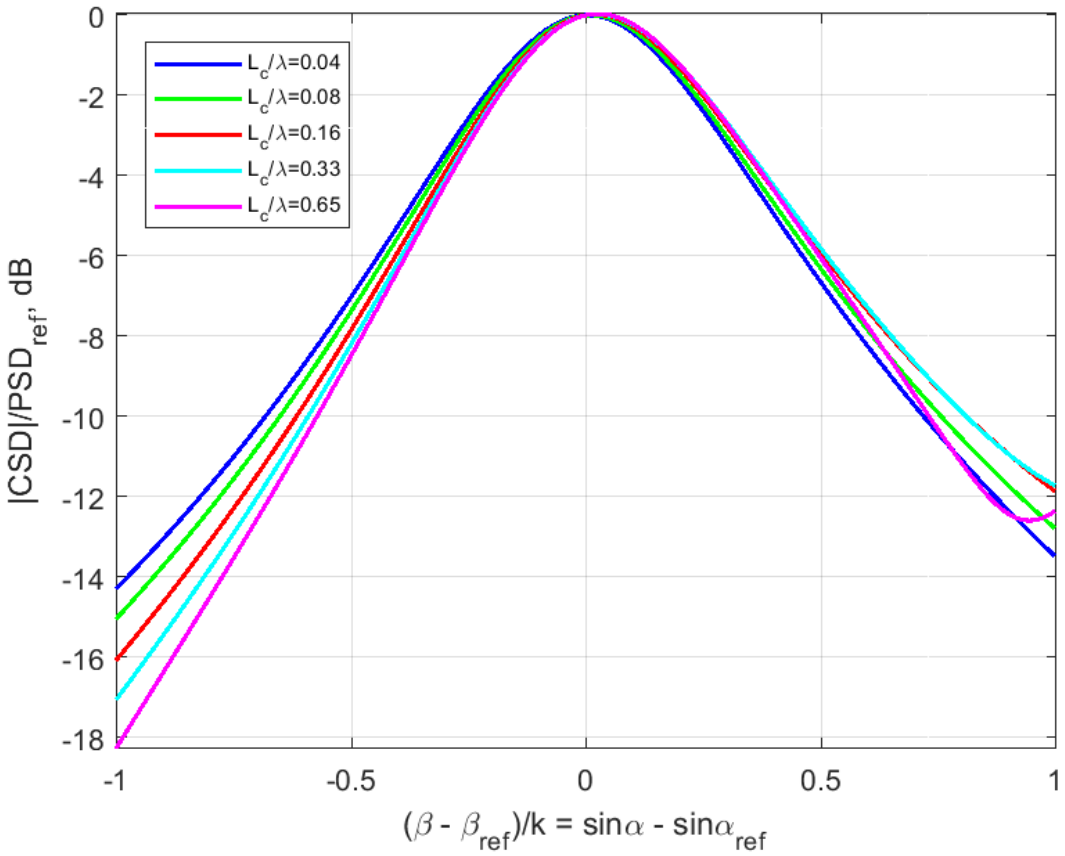

Figure 2c: Far-field CSD modulus, St = 0.1, Mc=0.6.

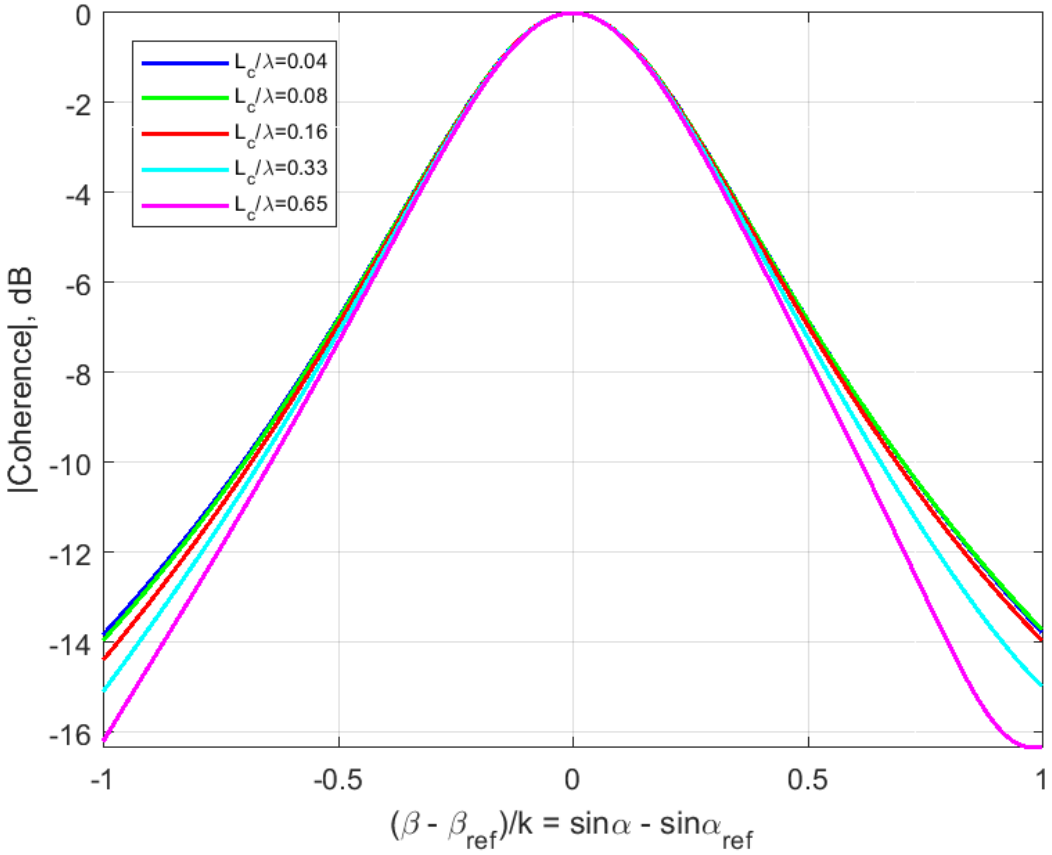

Figure 2d: Coherence modulus, St = 0.1, Mc=0.6.

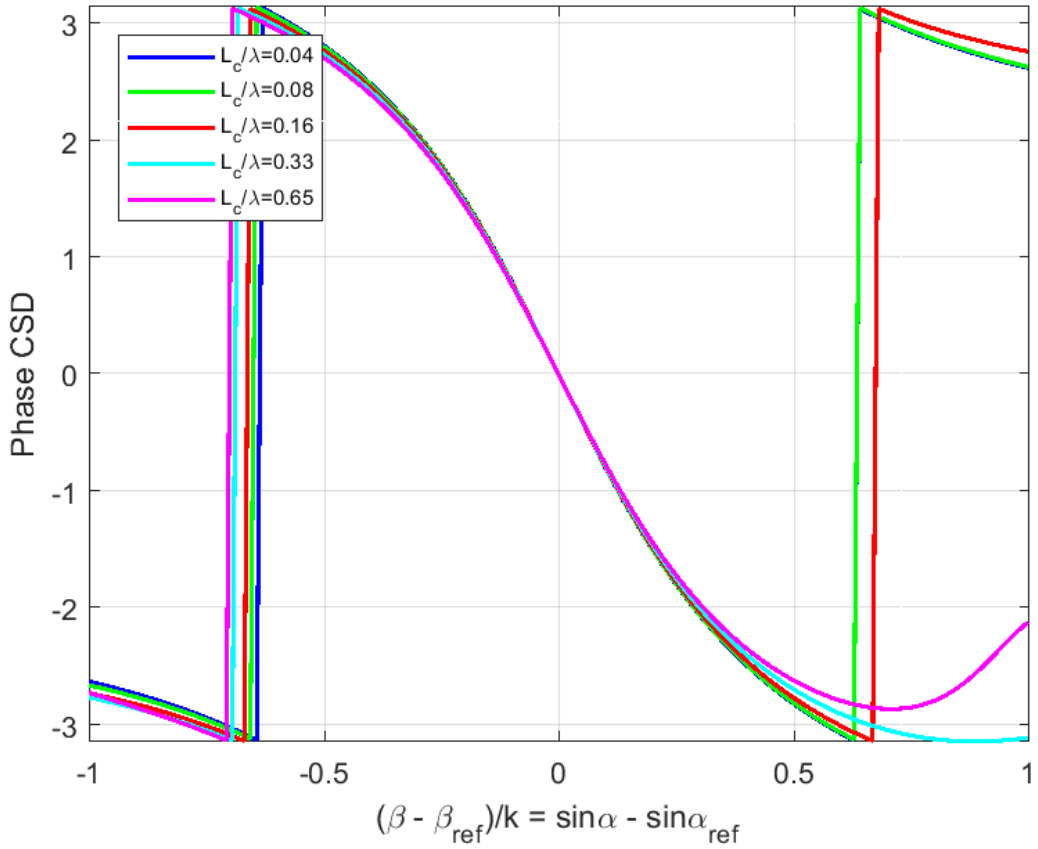

Figure 2e CSD phase, St = 0.1, Mc=0.6.

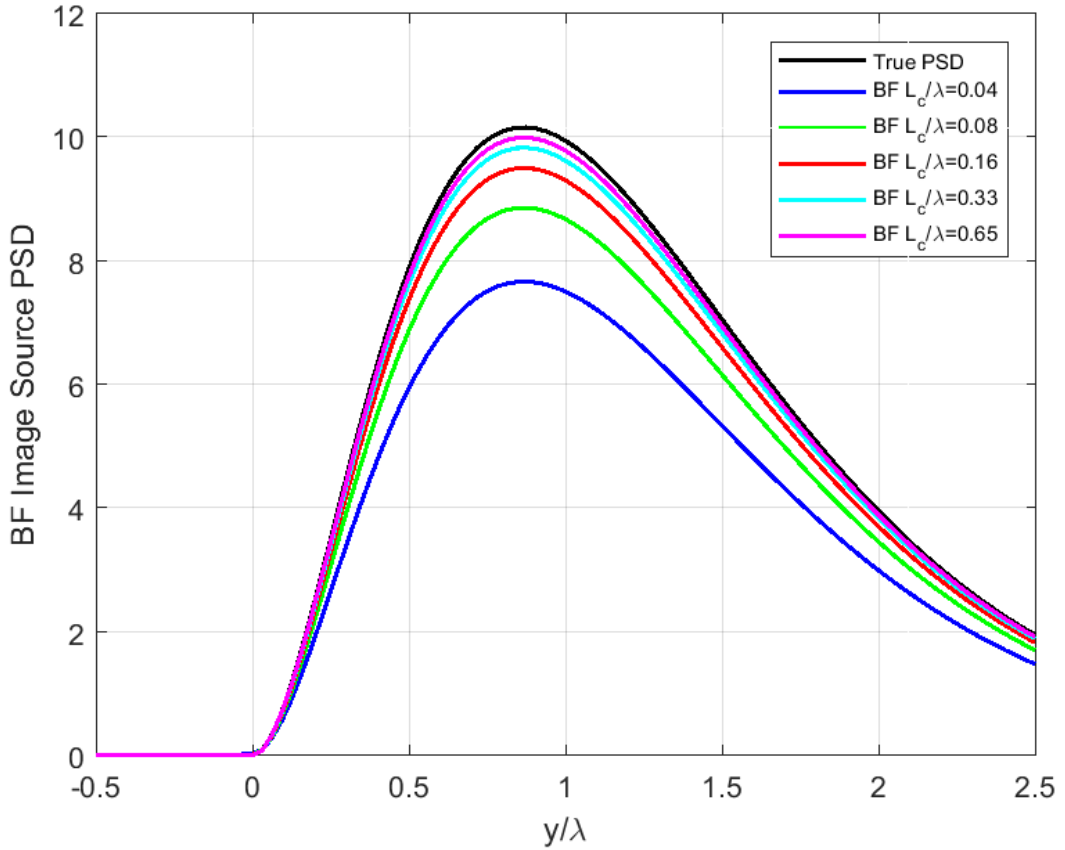

Figure 3a: BF Image of source PSD v. true source PSD, St=0.1, Mc=0.6, β_{max} = 10k

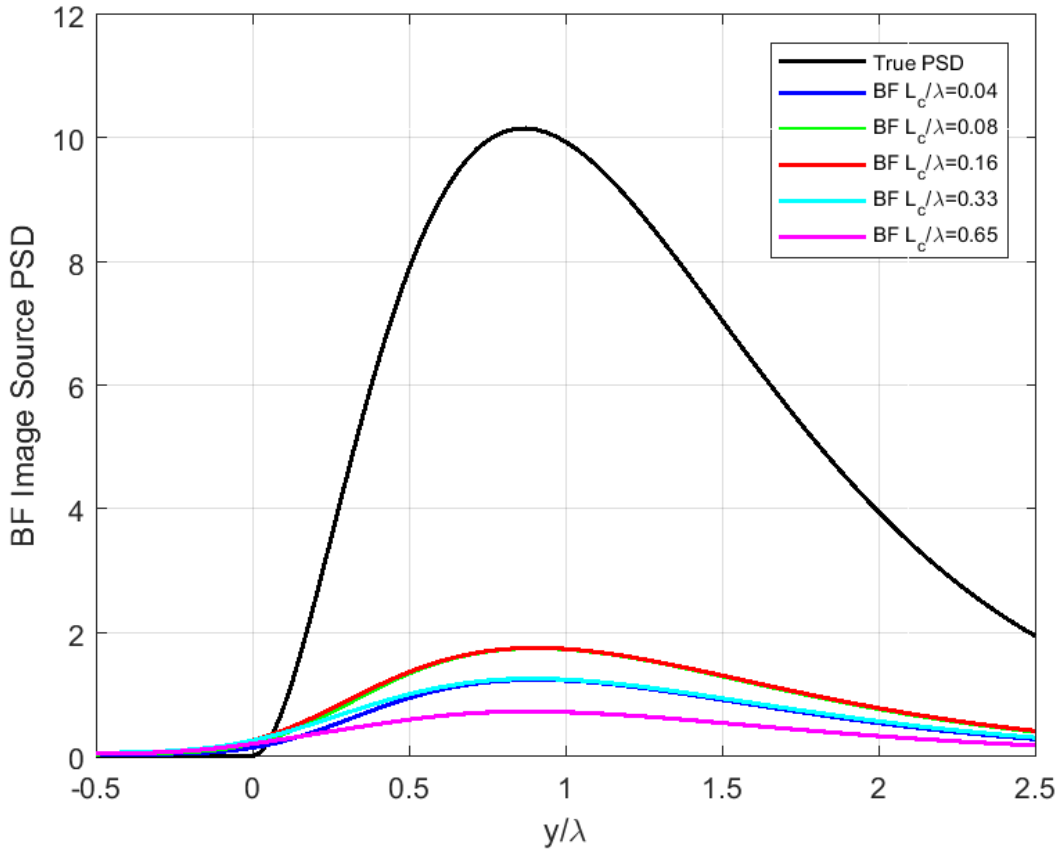

Figure 3b: BF Image of source PSD v. true source PSD, St=0.1, Mc=0.6, β_{max} = k

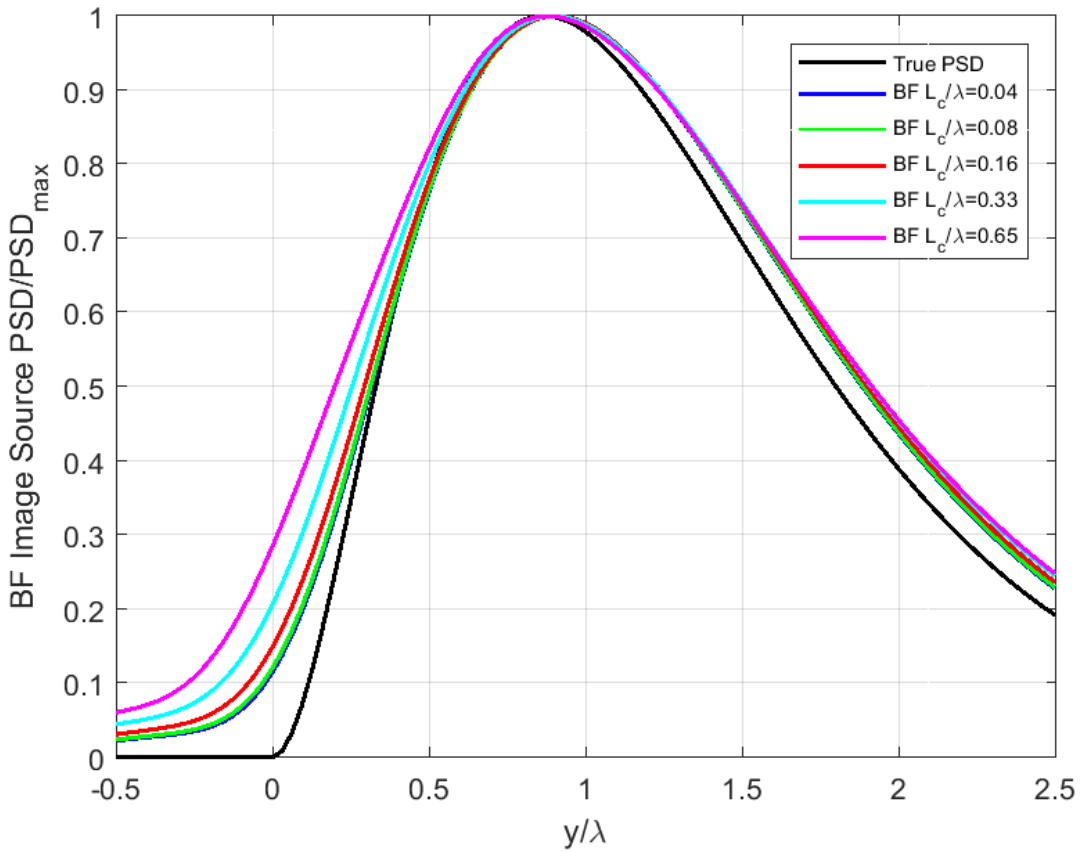

Figure 3c: Normalised BF image of source PSD v. true source PSD, St=0.1, Mc=0.6, β_{max} = k

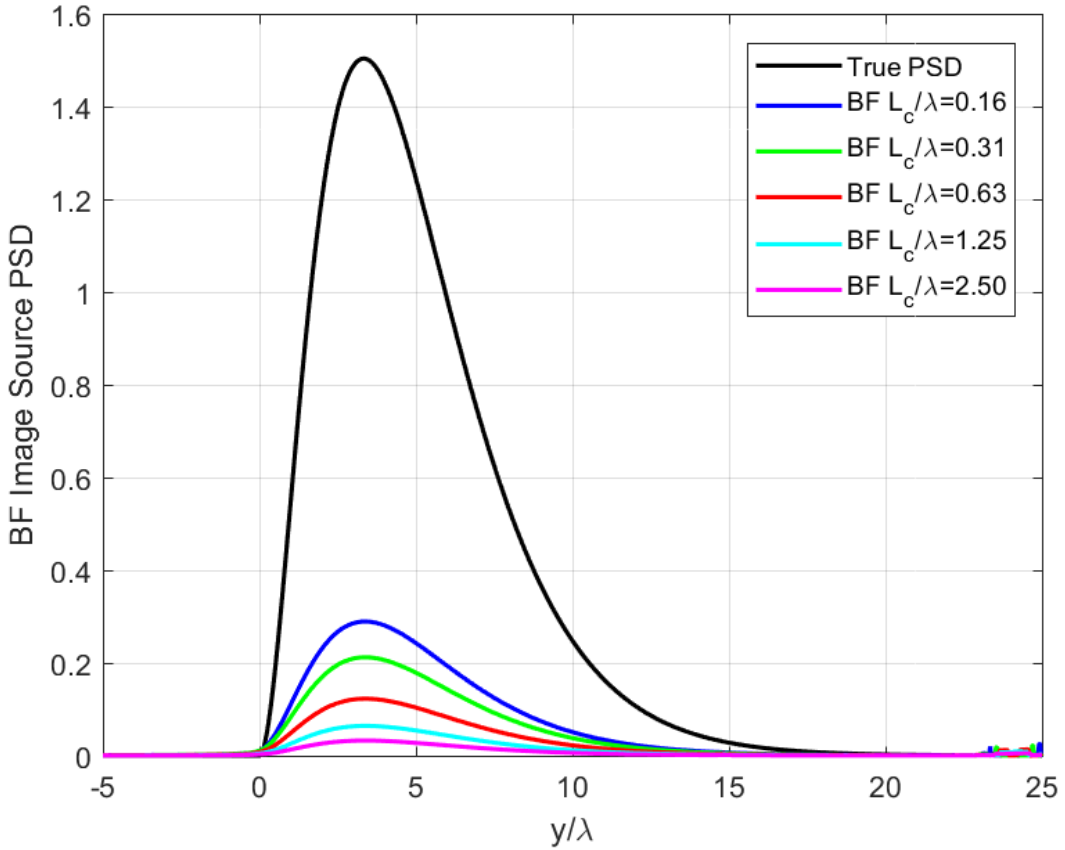

Figure 4a: BF Image of source PSD v. true source PSD, St=1, Mc=0.6, β_{max} = k

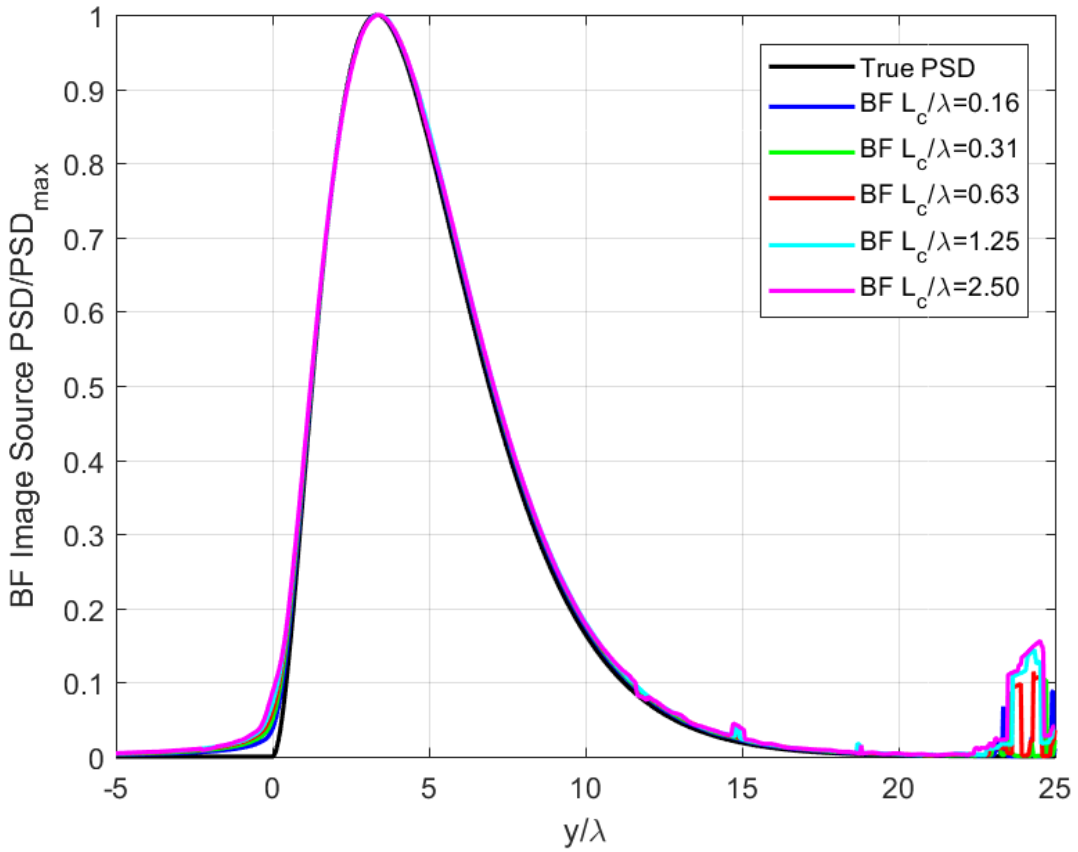

Figure 4b: Normalised BF image of source PSD v. true source PSD, St=1, Mc=0.6, $\beta_{max} = k$

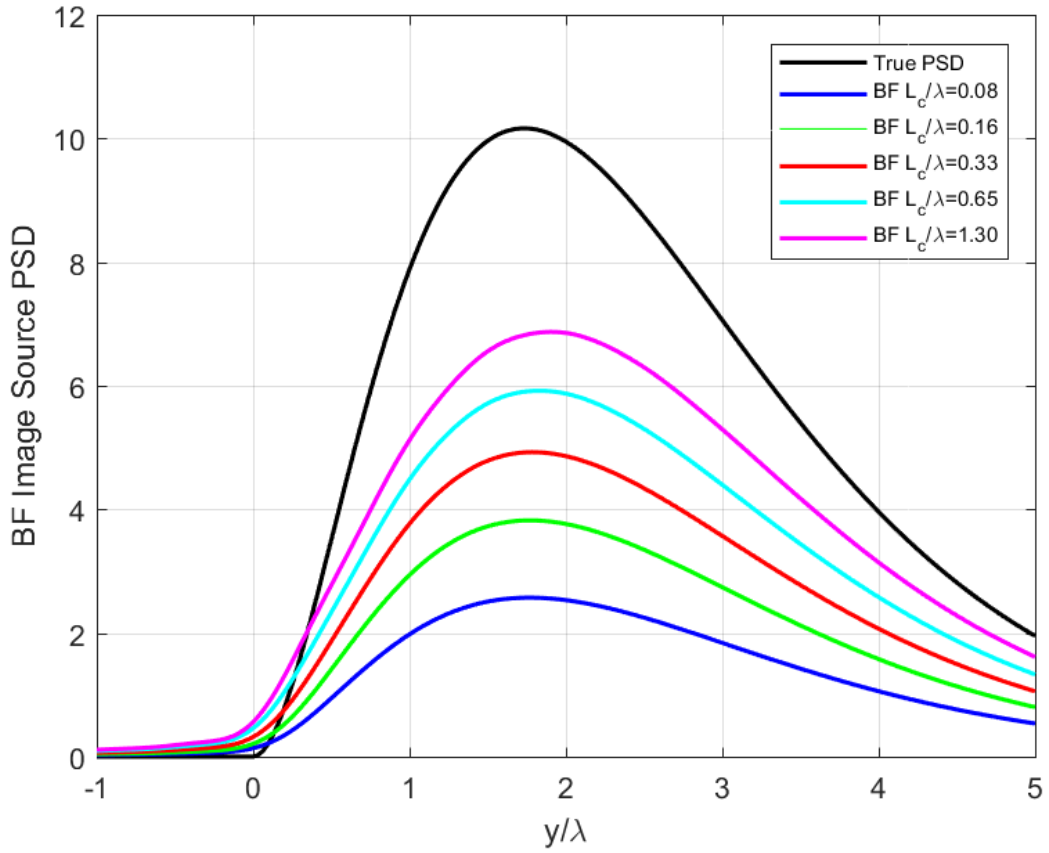

Figure 5: BF Image of PSD v. true PSD, St=0.1, M_c=1.2, β_{max} = k

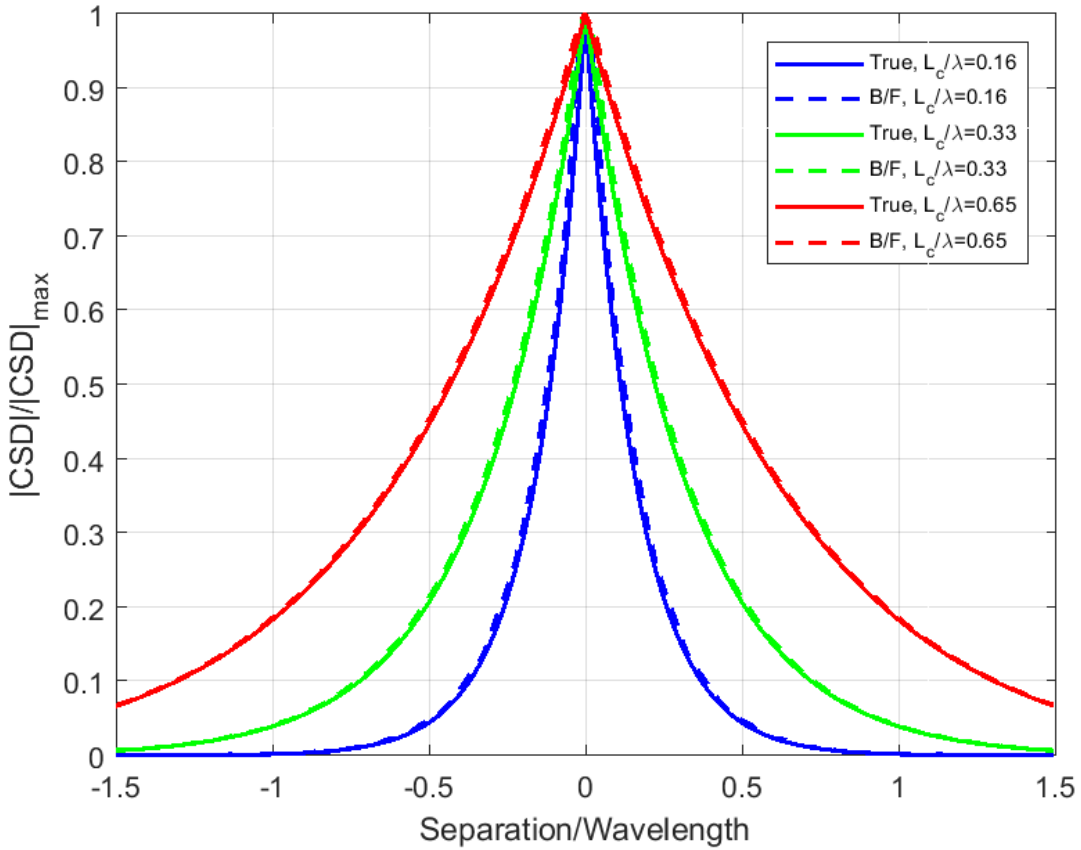

Figure 6a: BF Image of source |CSD| v. true source |CSD|, St=0.1, M_c=0.6, β_{max} = 10k

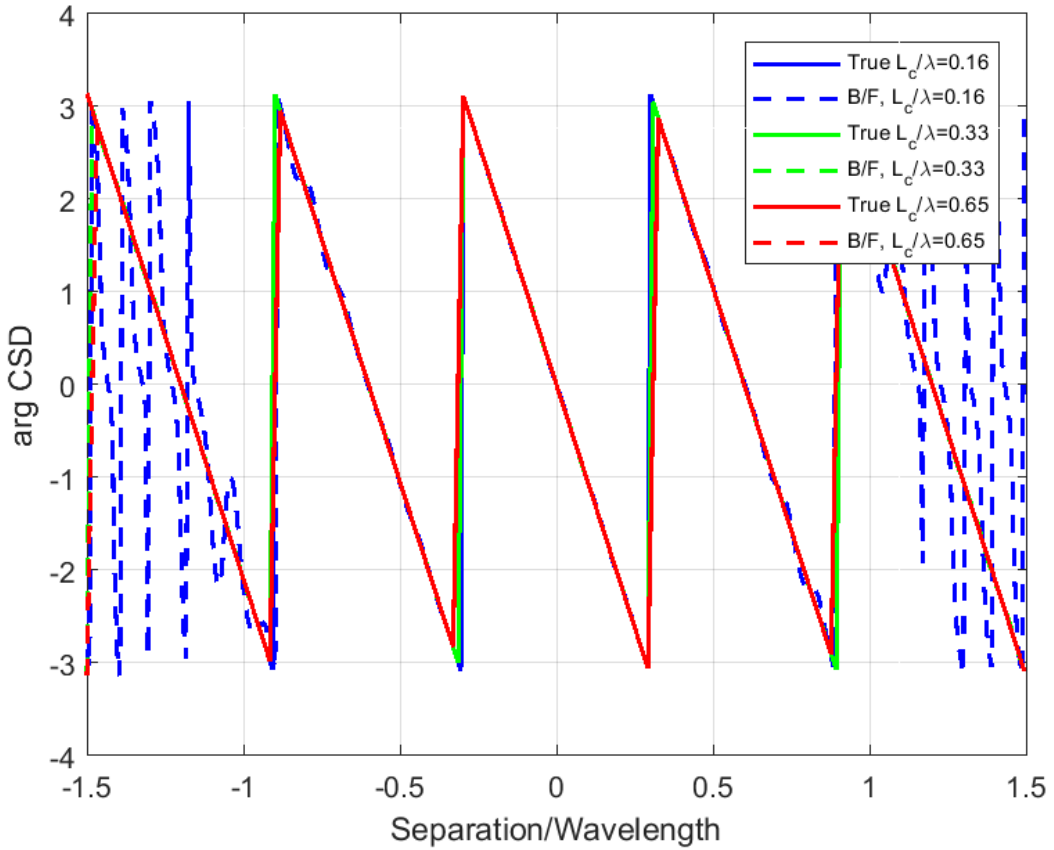

Figure 6b: BF Image of source CSD phase v. true source CSD phase, St=0.1, M_c=0.6, β_{max} = 10k

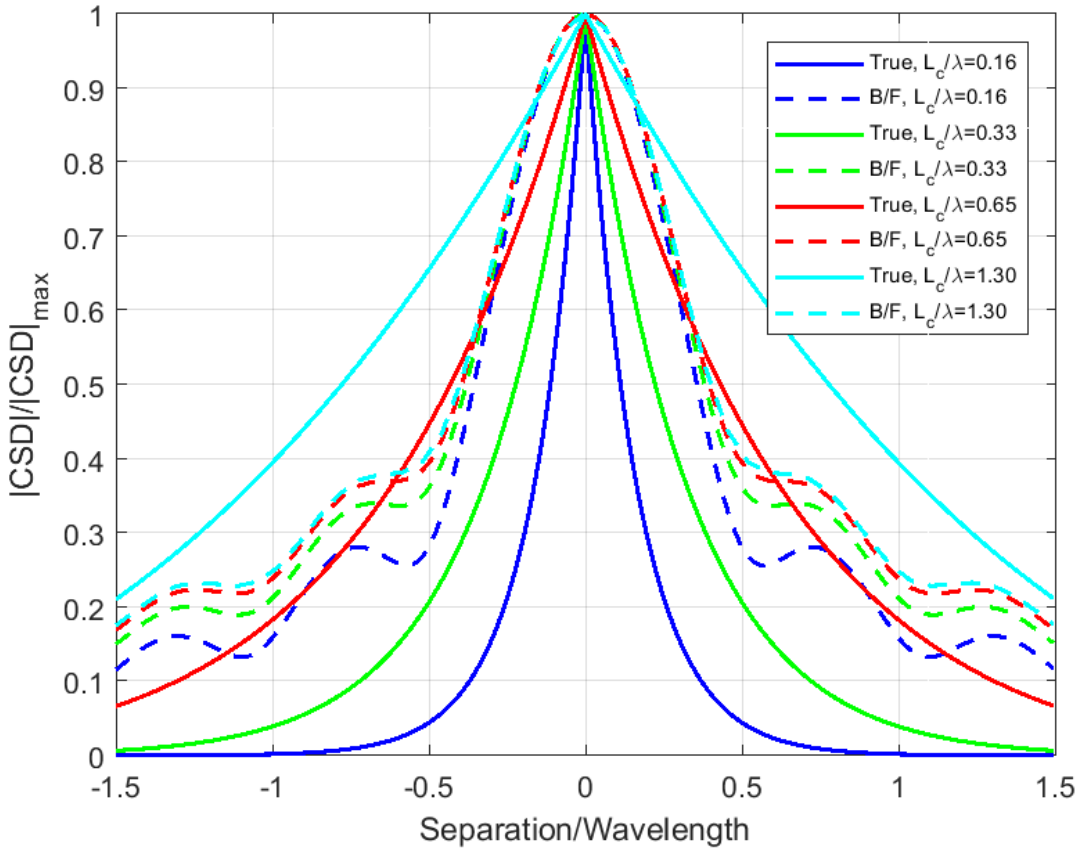

Figure 7a: BF Image of source |CSD| v. true source |CSD|, St=0.1, M_c=0.6, β_{max} = k

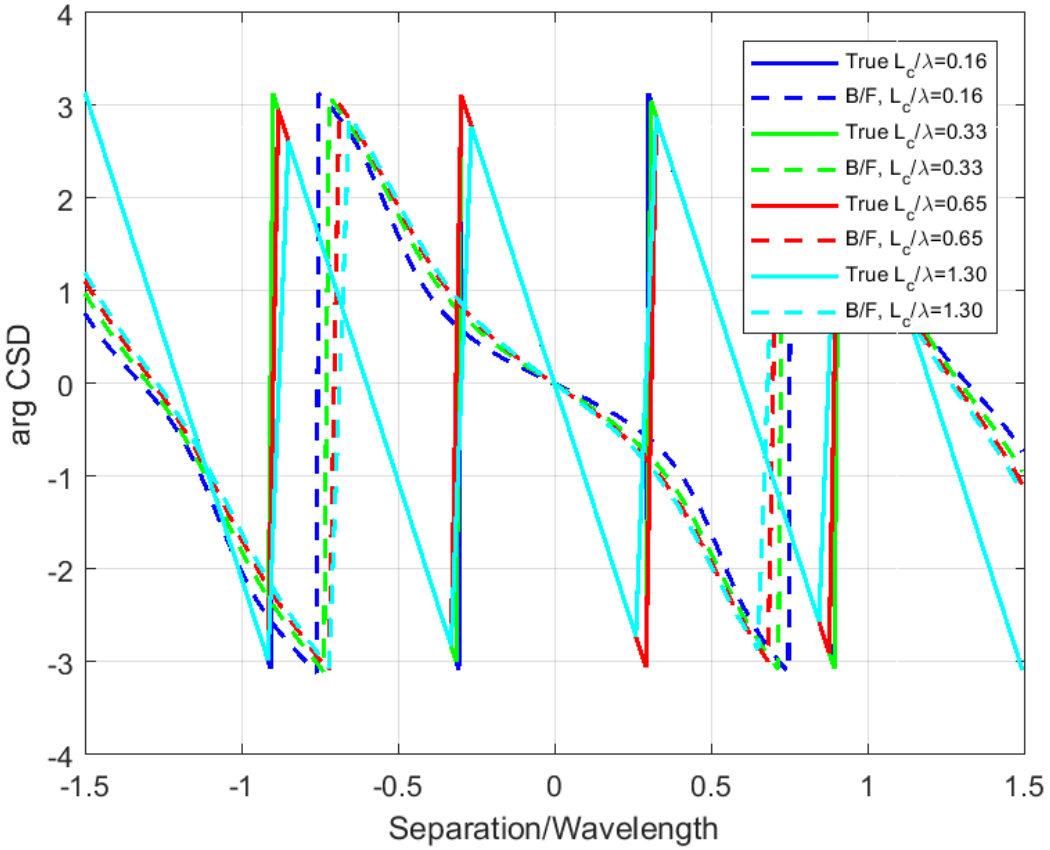

Figure 7b: BF Image of source CSD phase v. true source CSD phase, St=0.1, M_c=0.6, β_{max} = k

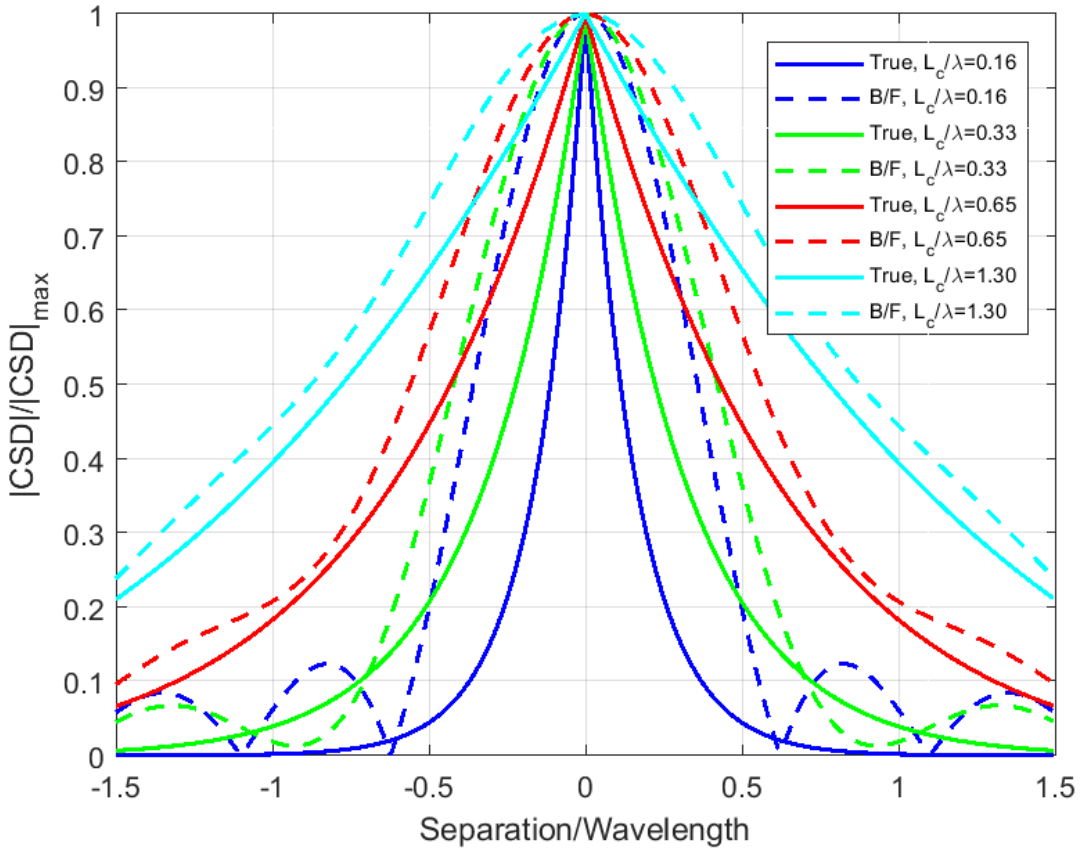

Figure 8: BF Image of source |CSD| v. true source |CSD|, St=0.1, M_c=0.0, β_{max} = k

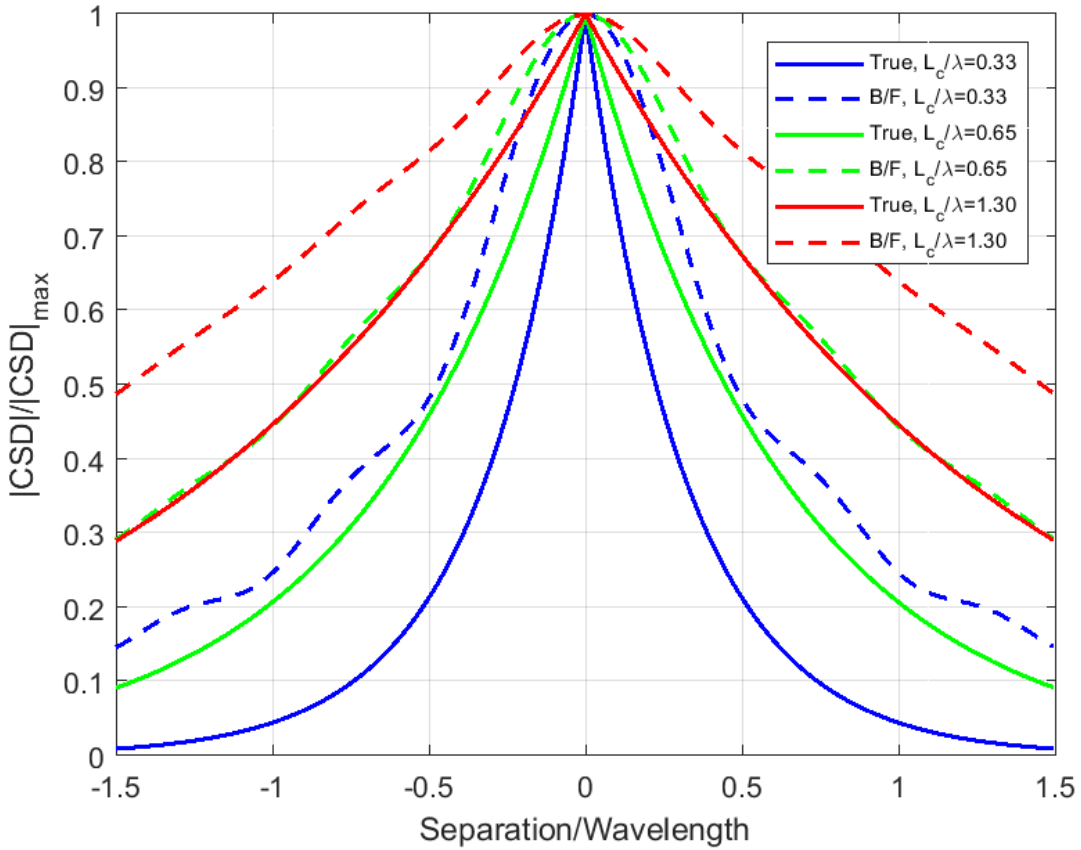

Figure 9a: BF Image of source |CSD| v. true source |CSD|, St=0.1, M_c=1.2, β_{max} = k

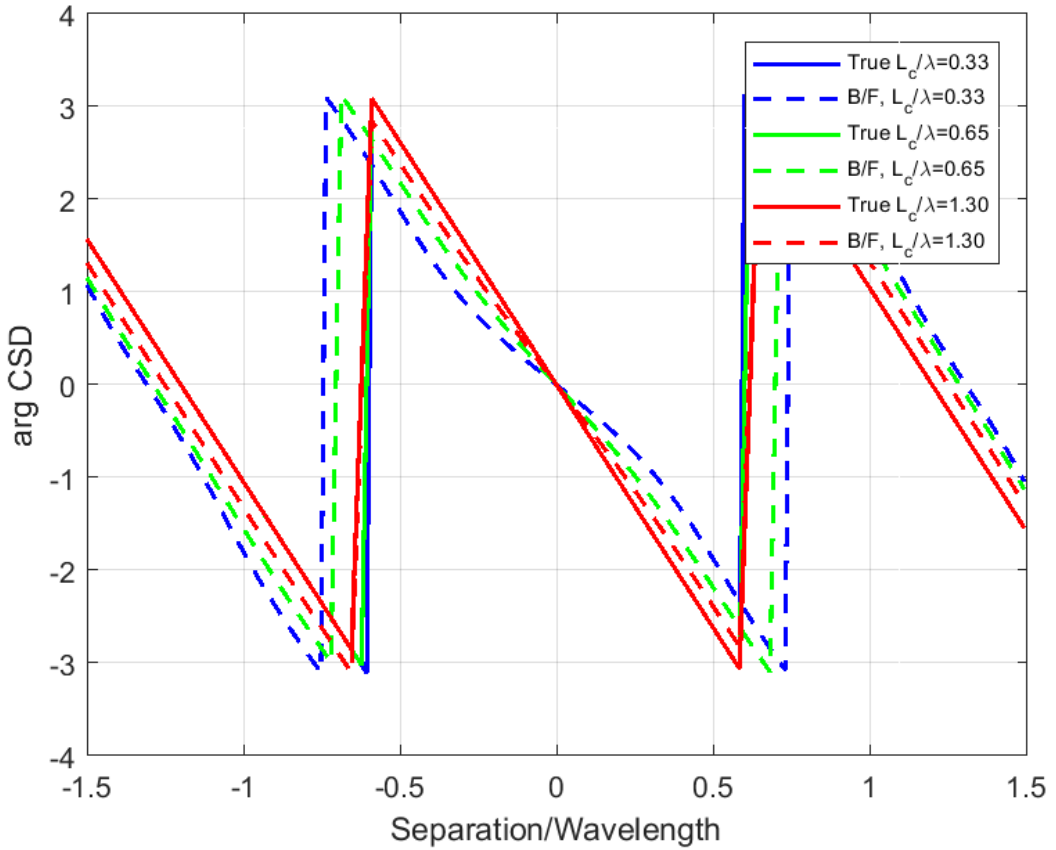

Figure 9b: BF Image of source CSD phase v. true source CSD phase, St=0.1, M_c=1.2, β_{max} = k

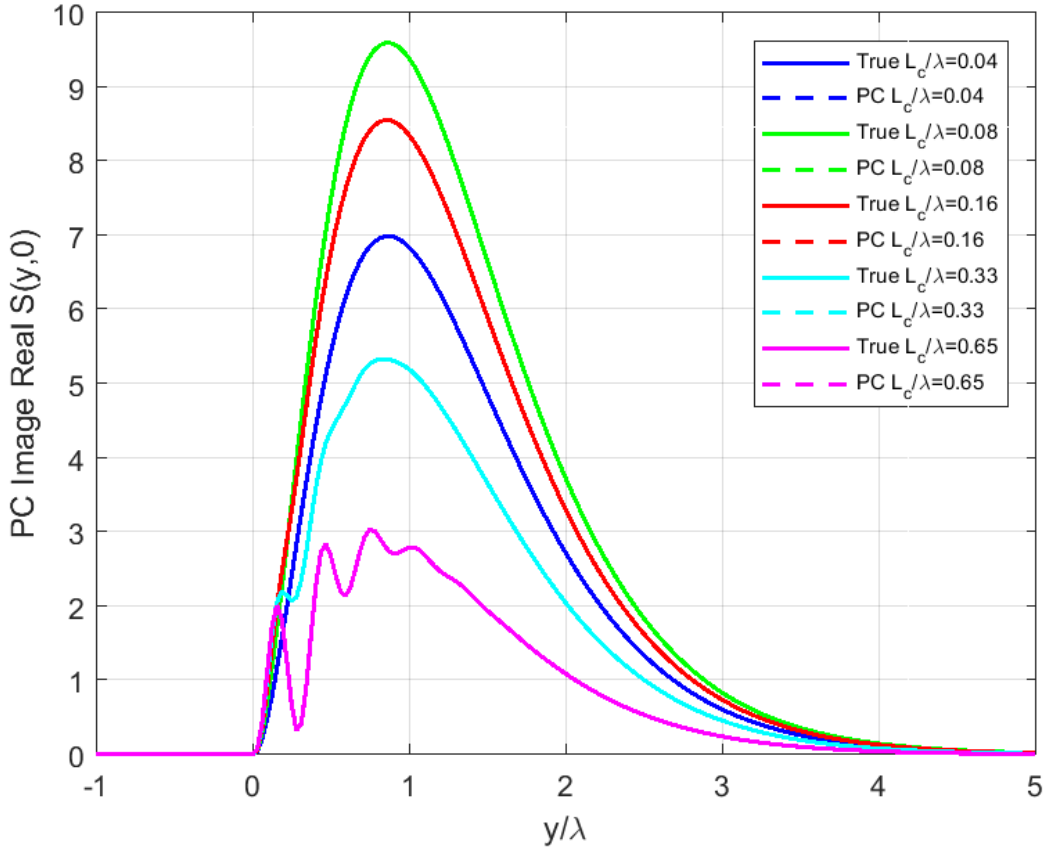

Figure 10a: PC image of source strength v. true source strength, St=0.1, M_c=0.6, β_{max} = 10k.

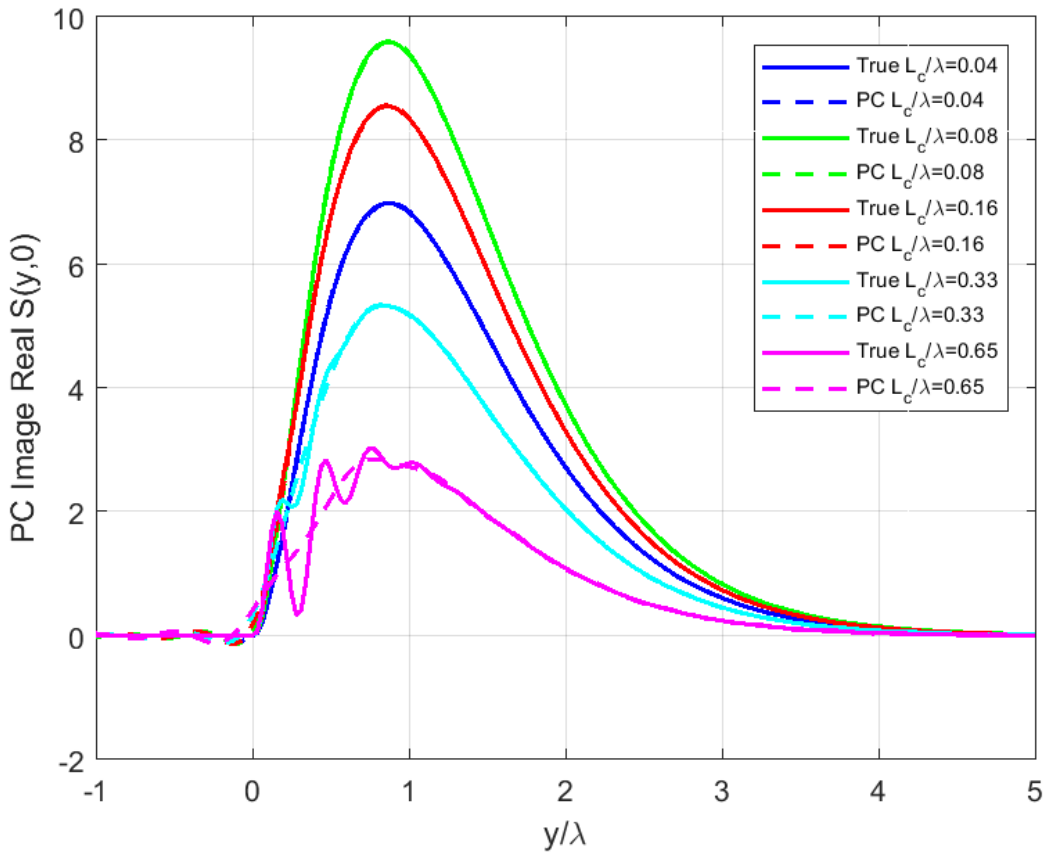

Figure 10b: PC image of source strength v. true source strength, St=0.1, M_c=0.6, β_{max} = k.

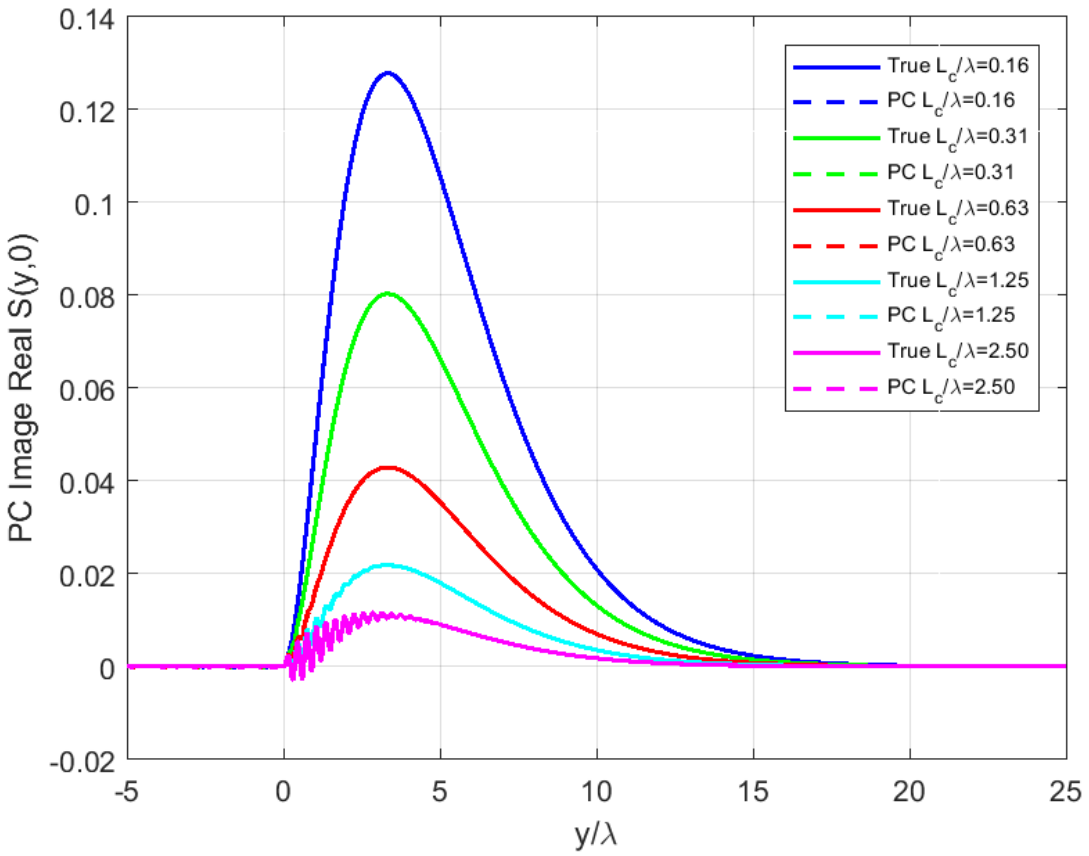

Figure 11: PC image of source strength v. true source strength, St=1, M_c=0.6, β_{max} = k.

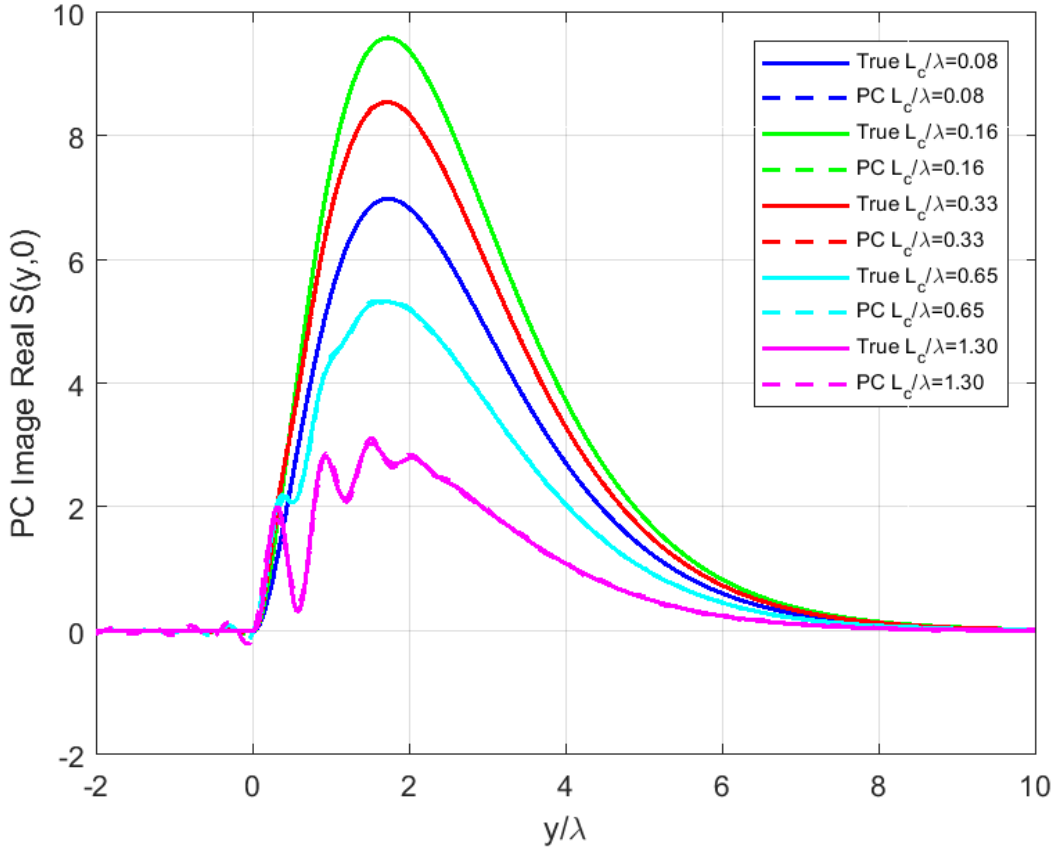

Figure 12: PC Image of source strength v. true source strength, St=0.1, M_c=1.2, β_{max} = k

References

[1] Billingsley, J. and Kinns, R., "The Acoustic Telescope," *Journal of Sound and Vibration*, Vol. 48, No.4, 1976, pp. 485-510.

[2] U. Michel 2006. AARC Engine noise phased array workshop, Cambridge, MA, USA. Characterization of jet noise with phased microphone arrays.

[3] Papamoschou, D., and Dadvar, A., "Localization of Multiple Types of Jet Noise Sources," AIAA Paper 2006-2644, May 2006.

[4] S. S. Lee 2006. AARC Engine noise phased array workshop, Cambridge, MA, USA. Phased-array measurements of jet noise source distributions.

[5] L. Brusniak, J. Underbrink and E. Nesbitt, D. Lynch and M. Martinez 2007. AIAA-2007-3612. Phased Array Measurements of Full- Scale Engine Exhaust Noise.

[6] J. Lan, J. Premo, G. Zlavog, and C. Breard 2007. AIAA-2007-3434. Phased Array Measurements of Full-Scale Engine Inlet Noise.

[7] M. Martinez 2007. AIAA-2007-3445. Microphone Polar Arc Phased Array for Locating Turbofan Source Noise Components.

[8] Dougherty R. and Mendoza, J. "Phased Array Beamforming with 100ft Polar Arc Microphones in a Static Engine Noise Test", AIAA Paper no 2008-0051, January 2008

[9] M. J. Fisher, M. Harper-Bourne and S. A. L. Glegg 1977. *J. Sound Vib.* 51(1), 23-54. Jet engine noise source location: the polar correlation technique.

[10] B. J. Tester and M. J. Fisher 1981 AIAA 81-2040 7th Aeroacoustics Conference, Palo Alto, CA, USA. Engine noise source breakdown: theory, simulation and results.

[11] Glegg, S. ""The Accuracy of Source Distributions Measured by Using Polar Correlation", Journal of Sound and Vibration, Vol. 80(l) pp. 3l-40, 1982

[12] P J R Strange, G Podmore, M J Fisher and B J Tester 1984. AIAA-84-2361. 9th AIAA/NASA Aeroacoustics Conference, Williamsburg, VA, USA. Coaxial jet noise source distributions.

[13] P. M. W. Pack and P. R. J. Strange1987. AIAA-87-2685 11th Aeroacoustics Conference, Palo Alto, CA, USA. Recent developments in source location.

[14] M. J. Fisher and K. R. Holland 1997. *J Sound Vib.* 201(1), 103-125. Measuring the relative strengths of a set of partially coherent acoustic sources.

[15] J. P. Battaner-Moro 2003. AIAA 2003-3324 9th AIAA/CEAS Aeroacoustics Conference, Hilton Head, SC, USA. New automated source breakdown algorithm for jet noise.

[16] B. J. Tester and S. A. L. Glegg 2008 14th AIAA/CEAS Aeroacoustics Conference, May 2009, Vancouver, USA. A review of engine noise source diagnostic methods for static engine tests, with phased array and polar correlation techniques.

[17] R. P. Dougherty and G. G. Podboy 2009. 15th AIAA/CEAS Aeroacoustics Conference, May 2009, Miami, USA. Improved Phased Array Imaging of a Model Jet.

[18] S. A. L. Glegg 1979. PhD thesis, Southampton University.

[19] C. K. W. Tam and L. Auriault 1999 *AIAA Journal*, 17, 145-153. Jet mixing noise from fine scale turbulence.

[20] S A Karabasov et al 2008. Using LES within an acoustic analogy approach for jet noise modelling. AIAA Paper No 2008-2985 *14th AIAA/CEAS Aeroacoustics Conference, Vancouver.*

[21] U. Michel and Funke 2008. AIAA2008-2860 14th Aeroacoustics Conference, Vancouver. Noise Source Analysis of an Aero engine with a New Inverse Method SODIX.

[22] T. F. Brooks and W. M. Humphreys 2006. *J. Sound Vib.* 294, 86-879. A deconvolution approach for mapping of acoustic sources (DAMAS) determined from phased microphone arrays.

[23] P. Sijtsma 2007. *Int. J. Aeroacoustics*, vol. 6, no. 4, pp 357-374. CLEAN based on spatial source coherence.